# Consistent lattice Boltzmann methods for incompressible axisymmetric flows

Liangqi Zhang,[1,2] Shiliang Yang,[1] Zhong Zeng,[2,3] Linmao Yin,[2] Ya Zhao,[1] and Jia Wei Chew[1,4,*]

[1]*School of Chemical and Biomedical Engineering, Nanyang Technological University, Singapore 637459, Singapore*

[2]*Department of Engineering Mechanics, College of Aerospace Engineering, Chongqing University, Chongqing 400044, People's Republic of China*

[3]*State Key Laboratory of Coal Mine Disaster Dynamics and Control, Chongqing University, Chongqing 400044, People's Republic of China*

[4]*Singapore Membrane Technology Center, Nanyang Environment and Water Research Institute, Nanyang Technological University, Singapore 637141, Singapore*

(Received 12 May 2016; published 4 August 2016)

In this work, consistent lattice Boltzmann (LB) methods for incompressible axisymmetric flows are developed based on two efficient axisymmetric LB models available in the literature. In accord with their respective original models, the proposed axisymmetric models evolve within the framework of the standard LB method and the source terms contain no gradient calculations. Moreover, the incompressibility conditions are realized with the Hermite expansion, thus the compressibility errors arising in the existing models are expected to be reduced by the proposed incompressible models. In addition, an extra relaxation parameter is added to the Bhatnagar-Gross-Krook collision operator to suppress the effect of the ghost variable and thus the numerical stability of the present models is significantly improved. Theoretical analyses, based on the Chapman-Enskog expansion and the equivalent moment system, are performed to derive the macroscopic equations from the LB models and the resulting truncation terms (i.e., the compressibility errors) are investigated. In addition, numerical validations are carried out based on four well-acknowledged benchmark tests and the accuracy and applicability of the proposed incompressible axisymmetric LB models are verified.

DOI: 10.1103/PhysRevE.94.023302

## I. INTRODUCTION

Axisymmetric fluid flow and heat and mass transfer in cylindrical systems are widely encountered in engineering practices. Taking advantage of the axisymmetric condition, the three-dimensional (3D) axisymmetric flow can be reduced to a quasi-2D problem in the meridian plane, which significantly reduces the computational requirements and avoids the curve boundary treatments. Therefore, although the 3D lattice Boltzmann (LB) method is more realistic and accurate for axisymmetric flow [1–3], much effort has been devoted to developing 2D axisymmetric LB models [4–11].

Specifically, the existing axisymmetric LB models are divided into two categories: the bottom-up models and the top-down models. In the bottom-up models, the LB equation and the equilibrium distribution functions are designed sequentially and thus the effect of axisymmetry is considered at the distribution function level. In particular, starting from the axisymmetric Boltzmann equation, a kinetic theory based model was proposed by Guo *et al.* [10], in which reduced distribution functions were defined in the meridian plane and the corresponding equilibrium distribution functions were directly derived from the Maxwellian equilibrium distribution. The LB equations in Ref. [10] were directly the discrete evolution equations for the reduced distribution functions. It has been proven that the axisymmetric Navier-Stokes (NS) equations can be derived from the Guo *et al.* [10] model and all the velocity components were described in the same fashion. Moreover, the source terms were directly derived from the relevant parts of the evolution equations for the reduced distribution functions and contained no velocity gradient terms. The above explicit kinetic theory origin confers on the Guo *et al.* [10] model a solid physics basis and makes it easy for generalization. The Guo *et al.* [10] model and its derivative models have achieved successful application for various axisymmetric flows [12–17].

As for the top-down models, coordinate system transformations are performed such that the axisymmetric NS equations in the cylindrical system are reformulated as pseudo-Cartesian ones. The extra terms caused by the coordinate transformations are regarded as source terms and are directly added to the standard LB equation. Therefore, the top-down models are developed within the framework of the conventional LB method and axisymmetric conditions are realized at the macroscopic level. In this regard, the LB method is used as a numerical solver for the Cartesian macroscopic convection diffusion equations. The first axisymmetric LB model was proposed by Halliday *et al.* [4] in the top-down fashion, which led to incorrect momentum equations with a missing term related to the radial velocity component. Afterward, Lee *et al.* [5] and Reis and Phillips [6,18,19] proposed improved models and accurate macroscopic equations were obtained. As discussed by Huang and Lu [20], although the two improved models were developed independently, they were proven to be basically identical. Based on the model proposed by Halliday *et al.* [4], a hybrid method was developed by Peng *et al.* [21] for axisymmetric rotating thermal flows and subsequently the numerical stability was improved by Huang *et al.* [22]. In addition, the Halliday *et al.* [4] model was also extended for application to multiphase flows by Premnath and Abraham [23]. However, as claimed by Zhou [8], the above top-down models suffered from the complicated source terms. In particular, the forcing source term contained more than ten items in the improved models when the missing term in the model of Halliday *et al.* [4] was added. In order to

*Author for correspondence: jchew@ntu.edu.sg

 

simplify the source terms, Chen *et al.* [24,25] proposed an alternative axisymmetric LB model based on the vorticity stream equation. Although the source terms in the Chen *et al.* [24,25] model were simpler, the model had to solve a Poisson equation at each time step and the vorticity at the boundary was hard to determine, thus its computation efficiency was highly compromised. Furthermore, an efficient model was proposed by Zhou [8], in which the source terms were simply the extra terms in the transformed pseudo-Cartesian equations and the centered scheme was applied to remove the discrete lattice effects.

It should be noted that velocity gradient terms exist in the extra terms due to the coordinate transformation, which leads to additional finite-difference calculations in the above-mentioned top-down LB models [4–6,8,18,23,26,27]. In the axisymmetric thermal model proposed by Li *et al.* [28], the concept of evaluating the temperature gradient terms with the nonequilibrium part of the distribution function was proposed and then applied to the general hydrodynamic equations [7]. The Zhou [8] model was subsequently revised by incorporating the idea the Li *et al.* model [28] and the revised model was then extended to the application of general axisymmetric convection-diffusion equations [29] and even axisymmetric compressible flows with low Mach number Ma [30]. Therefore, the improved axisymmetric model proposed by Li *et al.* [7] and the revised model by Zhou [9], as well as their derivative models, are the most efficient top-down models to date, since the source terms are simple and the gradient calculations are avoided. However, as demonstrated in the Chapman-Enskog analysis, the derived macroscopic equations from the two models are compressible and thus compressibility errors arise when incompressible axisymmetric flows are considered.

In this work, incompressible LB models for axisymmetric flows are proposed within the framework of the two efficient top-down models [7,9] and thus consistent LB methods for incompressible axisymmetric flows are developed. Incompressibility conditions are directly introduced by revising the moment equations of the standard LB model and then the equilibrium distribution functions and the relevant source terms are obtained from the revised moments by using the Hermite tensorial polynomials [31–33]. In addition, a set of computing formulas for the macroscopic variables is proposed in accord with the modified moment equations. In particular, the pressure formula in the present models is derived from the second-order moment of the distribution function with the moment of the nonequilibrium part obtained from the Chapman-Enskog analysis. In addition, starting from the ideas of the multiple-relaxation-time (MRT) model [34–36] and the regularized lattice Bhatnagar-Gross-Krook (RLBGK) model [37,38], an additional relaxation parameter pertaining to the "ghost" variables is added to the Bhatnagar-Gross-Krook (BGK) collision operator, which highly enhances the numerical stability of the present models while having no effect on the evolution of the hydrodynamic variables. The present incompressible models retain the advantages from their corresponding original counterparts in that they are consistent with the conventional LB method and the source terms are simple and contain no gradient terms. Moreover, the recovered macroscopic equations and the order of the compressibility errors of the involved LB models are analyzed theoretically with the Chapman-Enskog analysis and the equivalent moment system in the diffusive scaling [39]. Furthermore, numerical validations for the present models are carried out with various test cases. It is demonstrated that the numerical results from the present models agree well with the reference solutions, and the compressibility errors in the Li *et al.* model [7] and the revised Zhou [9] model are effectively reduced.

## II. FORMULATIONS

### A. Coordinate transformations of the macroscopic equations

The macroscopic equations for incompressible axisymmetric flows in cylindrical coordinate system are given as

$$\frac{\partial u_j}{\partial x_j} + \frac{u_r}{r} = 0, \tag{1a}$$

$$\rho\left[\frac{\partial u_i}{\partial t} + \frac{\partial}{\partial x_j}(u_i u_j)\right] = -\frac{\partial p}{\partial x_i} + \mu\frac{\partial^2}{\partial x_j \partial x_j}u_i + \frac{\mu}{r}\frac{\partial u_i}{\partial r} - \frac{\mu u_r}{r^2}\delta_{ir} - \frac{\rho u_i u_r}{r}, \tag{1b}$$

where $i$ and $j$ denote, respectively, the $r$ and $z$ coordinates in the meridian plane and $\rho$, $u_i$, $p$, and $\mu$ are, respectively, the fluid density, velocity, pressure, and dynamic viscosity. With the following relation derived from the incompressibility continuity equation (1a):

$$\mu\frac{\partial^2 u_i}{\partial x_j \partial x_j} = \frac{\partial}{\partial x_j}\left[\mu\left(\frac{\partial u_i}{\partial x_j} + \frac{\partial u_j}{\partial x_i}\right)\right] + \frac{\mu}{r}\frac{\partial u_r}{\partial x_i} - \frac{\mu u_r}{r^2}\delta_{ir}, \tag{2}$$

the momentum equation (1b) is represented in a pseudo-Cartesian coordinate system as

$$\rho\left[\frac{\partial u_i}{\partial t} + \frac{\partial}{\partial x_j}(u_i u_j)\right] = -\frac{\partial p}{\partial x_i} + \frac{\partial}{\partial x_j}\left[\mu\left(\frac{\partial u_i}{\partial x_j} + \frac{\partial u_j}{\partial x_i}\right)\right] + \frac{\mu}{r}\left(\frac{\partial u_i}{\partial r} + \frac{\partial u_r}{\partial x_i}\right) - \frac{2\mu u_r}{r^2}\delta_{ir} - \frac{\rho u_i u_r}{r}, \tag{3}$$

while the macroscopic equations derived from the standard LB equation are of the form

$$\frac{\partial}{\partial t}\rho + \frac{\partial}{\partial x_j}(\rho u_j) = 0, \tag{4a}$$

$$\frac{\partial}{\partial t}(\rho u_i) + \frac{\partial}{\partial x_j}(\rho u_i u_j) = -\frac{\partial p}{\partial x_i} + \frac{\partial}{\partial x_j}\left[\mu\left(\frac{\partial u_i}{\partial x_j} + \frac{\partial u_j}{\partial x_i}\right)\right]. \tag{4b}$$

Therefore, comparing Eq. (4b) with Eq. (3), the extra terms in the latter are treated as source terms and the standard LB method can be applied to describe the incompressible axisymmetric flows.

### B. Review on two efficient top-down axisymmetric LB models

#### 1. Li et al. model

A modified LB equation was proposed in the Li *et al.* [7] model

$$\begin{aligned} & f_\alpha(\boldsymbol{x}+\boldsymbol{\xi}_\alpha\delta t, t+\delta t) - f_\alpha(\boldsymbol{x},t) \\ &= \frac{\delta t}{2}\left[\Omega_\alpha|_{(\boldsymbol{x},t)} + \Omega_\alpha|_{(\boldsymbol{x}+\boldsymbol{\xi}_\alpha\delta t, t+\delta t)}\right] \\ &\quad + \frac{\delta t}{2}\left[S_\alpha|_{(\boldsymbol{x},t)} + S_\alpha|_{(\boldsymbol{x}+\boldsymbol{\xi}_\alpha\delta t, t+\delta t)}\right] \\ &\quad - \delta t\frac{\xi_{\alpha r}}{r}\left(f_\alpha - f_\alpha^{(\mathrm{eq})}\right)|_{(\boldsymbol{x},t)}, \end{aligned} \tag{5}$$

where $\Omega_\alpha = -\frac{1}{\tau_f}(f_\alpha - f_\alpha^{(\mathrm{eq})})$ is the BGK collision operator and $\tau_f$ is the single relaxation time [7]. Notably, the above equation is directly derived from the trapezium rule based time discretization of the discrete Boltzmann equation. In addition, the last term on the right-hand side of Eq. (5) is an innovative way of representing the velocity gradients in the source terms of Eq. (3). The remaining source terms in Eq. (3) are related to $S_\alpha$ in Eq. (5) by

$$S_\alpha = \left[\frac{(\xi_{\alpha i} - u_i)F_i}{\rho RT} - \frac{u_r}{r}\right] f_\alpha^{(\mathrm{eq})}, \quad F_i = -\frac{2\mu u_r}{r^2}\delta_{ir}, \tag{6}$$

where $R$ is the ideal gas constant, $T$ is the fluid temperature, and $RT = c_s^2$ is constant for isothermal flows. The equilibrium distribution function in Eq. (5) is consistent with that of the standard LB model

$$f_\alpha^{(\mathrm{eq})} = \rho w_\alpha\left[1 + \frac{\boldsymbol{u}\cdot\boldsymbol{\xi}_\alpha}{RT} + \frac{(\boldsymbol{u}\cdot\boldsymbol{\xi}_\alpha)^2}{2(RT)^2} - \frac{\boldsymbol{u}^2}{2RT}\right], \tag{7}$$

where $\boldsymbol{\xi}_\alpha$ and $w_\alpha$ are, respectively, the discrete particle velocity vectors and the corresponding weight coefficients of the D2Q9 lattice model:

$$\boldsymbol{\xi}_\alpha = \begin{cases} (0,0), & \alpha = 0 \\ c\{\cos[(\alpha-1)\pi/2], \sin[(\alpha-1)\pi/2]\}, & \alpha = 1,2,3,4 \\ \sqrt{2}c\{\cos[(2\alpha-1)\pi/4], \sin[(2\alpha-1)\pi/4]\}, & \alpha = 5,6,7,8, \end{cases} \tag{8a}$$

$$w_0 = 4/9, \quad w_{1,2,3,4} = 1/9, \quad w_{5,6,7,8} = 1/36. \tag{8b}$$

The lattice speed $c$ in Eq. (8a) is defined as $c = \delta x/\delta t$ and is related to $c_s$ by $c = \sqrt{3}c_s$ and $\delta x$ and $\delta t$ are, respectively, the spatial and time steps. For the convenience of numerical implementation, the implicitness in Eq. (5) is eliminated by reconstructing the distribution function

$$\hat{f}_\alpha = f_\alpha - \frac{\delta t}{2}(\Omega_\alpha + S_\alpha) \tag{9}$$

and the evolution equation for $\hat{f}_\alpha$ is obtained from Eq. (5) as

$$\begin{aligned} & \hat{f}_\alpha(\boldsymbol{x}+\boldsymbol{\xi}_\alpha\delta t, t+\delta t) - \hat{f}_\alpha(\boldsymbol{x},t) \\ &= -\omega_\alpha\left[\hat{f}_\alpha(\boldsymbol{x},t) - f_\alpha^{(\mathrm{eq})}(\boldsymbol{x},t)\right] + \delta t\left(1 - \frac{\omega_\alpha}{2}\right)S_\alpha, \end{aligned} \tag{10}$$

where the relaxation parameter is related to the discrete particle velocity by

$$\omega_\alpha = \left(1 + \frac{\tau\delta t\xi_{\alpha r}}{r}\right)\Big/\left(\tau + \frac{1}{2}\right), \tag{11}$$

with $\tau = \tau_f/\delta t$ the dimensionless relaxation time. Then, with the moment equations of the original distribution function

$$\begin{aligned} \rho &= \sum_\alpha f_\alpha = \sum_\alpha f_\alpha^{(\mathrm{eq})}, \\ \rho u_i &= \sum_\alpha f_\alpha\xi_{\alpha i} = \sum_\alpha f_\alpha^{(\mathrm{eq})}\xi_{\alpha i}, \\ \rho u_i u_j + p\delta_{ij} &= \sum_\alpha f_\alpha^{(\mathrm{eq})}\xi_{\alpha i}\xi_{\alpha j}, \end{aligned} \tag{12}$$

the macroscopic variables are calculated from $\hat{f}_\alpha$ as

$$\begin{aligned} \rho &= \sum_\alpha \hat{f}_\alpha - \frac{\delta t}{2}\frac{\rho u_r}{r}, \\ \rho u_i &= \sum_\alpha \hat{f}_\alpha\xi_{\alpha i} - \frac{\delta t}{2}\left(\frac{\rho u_i u_r}{r} + \frac{2\mu u_r}{r^2}\delta_{ir}\right). \end{aligned} \tag{13}$$

In particular, the computing formula for the fluid velocity is further revised as

$$u_i = \frac{\sum_\alpha \hat{f}_\alpha\xi_{\alpha i}}{\sum_\alpha \hat{f}_\alpha + (\delta t\mu/r^2)\delta_{ir}}. \tag{14}$$

Then the Li *et al.* [7] model is extended to solve the axisymmetric convection-diffusion equation of the form

$$\frac{\partial(\rho\phi)}{\partial t} + \frac{\partial}{\partial x_j}(\rho\phi u_j) = \frac{\partial}{\partial x_j}\left(\lambda\frac{\partial\phi}{\partial x_j}\right) + \frac{\lambda}{r}\frac{\partial\phi}{\partial r} + \varphi, \tag{15}$$

where $\phi$ and $\lambda$ are, respectively, the scalar variable and the associated diffusion coefficient. Specifically, $\lambda$ is the thermal diffusion coefficient $\alpha$ when $\phi = T$ and $\lambda$ is the dynamic viscosity $\mu$ when $\phi = u_\theta$. The source term $\varphi$ is defined as

$$\varphi = \begin{cases} -\frac{\rho u_r}{r}T, & \phi = T \\ -\frac{2\rho u_\theta u_r}{r} - \frac{\mu u_\theta}{r^2}, & \phi = u_\theta. \end{cases} \tag{16}$$

With the D2Q4 lattice model

$$\boldsymbol{\xi}_k = c\{\cos[(k-1)\pi/2], \sin[(k-1)\pi/2]\}, \quad k = 1,2,3,4 \tag{17}$$

and the corresponding weight coefficient $w_k = 1/4$, the LB equation (10) is rewritten as

$$\hat{g}_k(\boldsymbol{x}+\boldsymbol{\xi}_k\delta t,t+\delta t)-\hat{g}_k(\boldsymbol{x},t) = -\omega_k[\hat{g}_k(\boldsymbol{x},t)-g_k^{(\mathrm{eq})}(\boldsymbol{x},t)]+\delta t\left(1-\frac{\omega_k}{2}\right)S_\alpha^g, \quad (18)$$

where $\hat{g}_k$ is the distribution functions accounting for $\phi$ and the diffusion coefficient is determined as $\lambda = \tau_g\delta t\rho RT'$ with $\omega_k = (1+\frac{\tau_g\delta t\xi_{kr}}{r})/(\tau_g+\frac{1}{2})$. The relevant equilibrium distribution $g_k^{(\mathrm{eq})}$ is defined as

$$g_k^{(\mathrm{eq})} = \rho\phi w_k\left(1+\frac{\boldsymbol{u}\cdot\boldsymbol{\xi}_k}{RT'}\right) \quad (19)$$

and $c_s' = \sqrt{RT'}$ in the D2Q4 lattice model is related to the lattice speed by $c = \sqrt{2}c_s'$. In addition, the discrete source term in Eq. (18) is expressed as

$$S_\alpha^g = w_k\varphi\left(1+\frac{\boldsymbol{u}\cdot\boldsymbol{\xi}_k}{RT'}\right). \quad (20)$$

The second-order velocity terms in Eq. (20) can be removed to improve the computation efficiency and such a simplification has been thoroughly validated by previous work [8,9,29]. Hence, Eq. (20) becomes

$$S_\alpha^g = w_k\varphi. \quad (21)$$

Finally, the azimuthal velocity component $u_\theta$ and the fluid temperature $T$ are derived from

$$\rho T = \sum_k \hat{g}_k - \rho\frac{u_r T\delta t}{2r}, \quad (22a)$$

$$\rho u_\theta = \sum_k \hat{g}_k - \frac{\delta t}{2}\left(\frac{2\rho u_\theta u_r}{r}+\frac{\mu u_\theta}{r^2}\right). \quad (22b)$$

If the rotation is involved, the source term in Eq. (6) should be further generalized as

$$F_i = -\left(\frac{2\mu u_r}{r^2}-\frac{\rho u_\theta^2}{r}\right)\delta_{ir}. \quad (23)$$

It should be noted that the macroscopic equations recovered from the Li *et al.* [7] model are compressible, as demonstrated by the Chapman-Enskog analysis in Appendix A, which may lead to compressibility errors since the incompressible continuity equation is necessary for the coordinate transformations from Eq. (1) to Eq. (3). In addition, another challenging issue is the calculation of the macroscopic variables that are coupled with each other and are hard to determine independently. In Ref. [7], the trapezium rule is not applied to the source term in the evolution of azimuthal velocity distribution function and a constant density $\rho_0$ is introduced. Thus, the macroscopic variable in Li *et al.* [7] is calculated in the following manner:

$$u_\theta = \sum_k \hat{g}_k/\rho_0 \quad \text{for } \phi = u_\theta, \quad (24a)$$

$$u_i = \frac{\sum_\alpha \hat{f}_\alpha\xi_{\alpha i}+\frac{\rho_0 u_\theta^2}{2r}\delta_{ir}}{\sum_\alpha \hat{f}_\alpha+(\delta t\rho_0\nu/r^2)\delta_{ir}}, \quad (24b)$$

$$\rho = \sum_\alpha \hat{f}_\alpha\Big/\left(1+\frac{\delta t}{2}\frac{u_r}{r}\right), \quad (24c)$$

$$T = \sum_k \hat{g}_k\Big/\rho_0\left(1+\frac{u_r\delta t}{2r}\right) \quad \text{for} \quad \phi = T. \quad (24d)$$

### 2. *Zhou model*

The LB equation adopted in the Zhou [9] model is given as

$$f_\alpha(\boldsymbol{x}+\boldsymbol{\xi}_\alpha\delta t,t+\delta t)-f_\alpha(\boldsymbol{x},t) = -\tau_\alpha\left(f_\alpha-f_\alpha^{(\mathrm{eq})}\right)\big|_{(\boldsymbol{x},t)}+w_\alpha\theta\delta t+\frac{w_\alpha}{RT}F_i\xi_{\alpha i}\delta t, \quad (25)$$

which differs from that of the Li *et al.* [7] model in that the time discretization is implemented by integrating along the characteristic line instead of the trapezium rule, hence the reconstructed distribution function in Eq. (9) is avoided, which is highly beneficial for simplifying the computation of the macroscopic variables [9]. Based on the idea in Ref. [7], an effective relaxation time is also introduced in Ref. [9] to reproduce the velocity gradient source terms

$$\tau_\alpha = \begin{cases}\frac{1}{\tau}, & r=0\\ \frac{1}{\tau}\left[1+\frac{(2\tau-1)\xi_{\alpha r}\delta t}{2r}\right], & r\neq 0.\end{cases} \quad (26)$$

The equilibrium distribution function defined in Eq. (7) is also applied in the Zhou [9] model. A distinct feature of the Zhou [9] model is that the source terms in Eq. (25) are defined as

$$\theta = -\frac{\rho u_r}{r}, \quad (27a)$$

$$F_i = -\frac{\rho u_i u_r}{r}-\frac{2\mu u_r}{r^2}\delta_{ir}, \quad (27b)$$

where $\theta$ and $F_i$ account for the source terms in, respectively, the continuity and momentum equations. In addition, the centered scheme is applied to remove the discrete lattice effects

$$\theta = \theta(\boldsymbol{x}+\boldsymbol{\xi}_\alpha\delta t/2,t+\delta t/2), \quad (28a)$$

$$F_i = F_i(\boldsymbol{x}+\boldsymbol{\xi}_\alpha\delta t/2,t+\delta t/2), \quad (28b)$$

which can be realized in any of the following ways with $\psi$ for either $\theta$ or $F_i$:

$$\psi(\boldsymbol{x}+\boldsymbol{\xi}_\alpha\delta t/2,t+\delta t/2) = \tfrac{1}{2}[\psi(\boldsymbol{x},t)+\psi(\boldsymbol{x}+\boldsymbol{\xi}_\alpha\delta t,t+\delta t)] \quad \text{(implicit)}, \quad (29a)$$

$$\psi(\boldsymbol{x}+\boldsymbol{\xi}_\alpha\delta t/2,t+\delta t/2) = \tfrac{1}{2}[\psi(\boldsymbol{x},t)+\psi(\boldsymbol{x}+\boldsymbol{\xi}_\alpha\delta t,t)] \quad \text{(semi-implicit)}, \quad (29b)$$

$$\psi(\boldsymbol{x}+\boldsymbol{\xi}_\alpha\delta t/2,t+\delta t/2) = \psi(\boldsymbol{x},t) \quad \text{(explicit)}. \quad (29c)$$

It should be noted that the implicit form of the centered scheme agrees exactly with the integration of the source term by the trapezium rule, which is the force scheme, proven to be free of the discrete lattice effects, proposed by Guo *et al.* [40]. However, iterations are necessary in practical simulations due to the implicitness of Eq. (29a). The explicit form is the most efficient but reduces the centered scheme to the direct force scheme, which suffers from the discrete lattice effects and the appearance of spurious terms in the resulting macroscopic equations [40]. Therefore, as a compromise between numerical efficiency and overall accuracy, the semi-implicit form in Eq. (29b) is adopted in the present work. Moreover, only the zeroth-order term for the first source term $w_\alpha\theta\delta t$ and

the first-order term for the second source term $\frac{w_\alpha}{RT}F_i\xi_{\alpha i}\delta t$ is considered in the Zhou [9] model, which has no effect on the order of the overall accuracy but makes the model more efficient.

As another advantage of the Zhou [9] model, the macroscopic variables are efficiently determined as

$$\rho = \sum_\alpha f_\alpha, \quad u_i = \sum_\alpha f_\alpha \xi_{\alpha i}/\rho. \tag{30}$$

It is demonstrated in the Chapman-Enskog analysis in Appendix B that the macroscopic equations recovered from the Zhou [9] model [i.e., Eq. (B6)] are consistent with those obtained from the Li *et al.* [7] model presented in Eq. (A10). However, a different definition of the kinematic viscosity is introduced as

$$\nu = \left(\tau - \tfrac{1}{2}\right)RT\delta t. \tag{31}$$

With the LB equation of the form

$$\begin{aligned} &g_k(\boldsymbol{x}+\boldsymbol{\xi}_k\delta t, t+\delta t) - g_k(\boldsymbol{x},t) \\ &\quad = -\tau_k\left(g_k - g_k^{(\mathrm{eq})}\right)\big|_{(\boldsymbol{x},t)} + w_k\theta^g\delta t \end{aligned} \tag{32}$$

and the equilibrium distribution function in Eq. (19), the Zhou [9] model can also be applied to solve the axisymmetric convection-diffusion equation (15). The relaxation parameter $\tau_k$ is determined as

$$\tau_k = \begin{cases} \frac{1}{\tau_g}, & r = 0 \\ \frac{1}{\tau_g}\left[1 + \frac{(2\tau_g-1)\xi_{kr}\delta t}{2r}\right], & r \neq 0, \end{cases} \tag{33}$$

where the diffusion coefficient $\lambda$ is related to $\tau_g$ as

$$\lambda = \left(\tau_g - \tfrac{1}{2}\right)RT'\delta t. \tag{34}$$

The source term in Eq. (32) is given as

$$\theta^g = \begin{cases} -\frac{\rho u_r}{r}T\big|_{(\boldsymbol{x}+\boldsymbol{\xi}_k\delta t/2, t+\delta t/2)}, & \phi = T \\ -\left(\frac{2\rho u_\theta u_r}{r} + \frac{\mu u_\theta}{r^2}\right)\big|_{(\boldsymbol{x}+\boldsymbol{\xi}_k\delta t/2, t+\delta t/2)}, & \phi = u_\theta. \end{cases} \tag{35}$$

Then the macroscopic scalar variables $T$ and $u_\theta$ are efficiently calculated as

$$u_\theta = \sum_k g_k/\rho \quad \text{for} \quad \phi = u_\theta, \tag{36a}$$

$$T = \sum_k g_k/\rho \quad \text{for} \quad \phi = T. \tag{36b}$$

Again, if the azimuthal velocity component is included, the forcing source term in Eq. (27b) should be revised as

$$F_i = -\frac{\rho u_i u_r}{r} - \frac{2\mu u_r}{r^2}\delta_{ir} + \frac{\rho u_\theta^2}{r}\delta_{ir}. \tag{37}$$

It is demonstrated that the Zhou [9] model share some similarities with the Li *et al.* [7] model in that both models are developed within the framework of the conventional standard LB model and no extra modifications are implemented on the LB equation and the relevant equilibrium distribution functions. In addition, the same idea for reproducing the velocity and scalar gradient source terms is adopted in both models. However, the centered scheme is adopted in Ref. [9] for the time discretization instead of the trapezium rule in Ref. [7]. As a direct consequence, the reconstructed distribution function is avoided in Ref. [9] and the calculations of the macroscopic variables are much simpler and more efficient. Furthermore, two factors lead to the difference in accuracy: (i) The semi-implicit form of the centered scheme in Eq. (29b), which is unable to avoid the discrete lattice effects completely, is adopted in Ref. [9] and (ii) the definitions of the source terms in Ref. [7] are more complete than those in Ref. [9]. The errors caused by these two factors are both of the same order as the truncation terms and thus the degree of the overall accuracy of Ref. [9] is not affected. Notably, the macroscopic equations derived from both models are compressible and inconsistent with the incompressible axisymmetric NS equations (1) and thus compressibility errors arise.

### C. Consistent LB methods for incompressible axisymmetric flows

In order to reduce the compressibility errors and derive the standard incompressible axisymmetric NS equations (1), the incompressibility conditions are incorporated into the two models reviewed above. More explicitly, the incompressible LB model proposed in our recent work [41,42] is extended to the application of the axisymmetric flows based on the framework provided by Li *et al.* [7] and Zhou [9].

#### *1. Equilibrium distribution function*

By assuming that the fluid density is a constant and the fluid pressure evolves independently, the moment equations of the continuous distributions are modified as

$$\begin{aligned} \rho_0 &= \int f\,d\boldsymbol{\xi} = \int f^{(\mathrm{eq})}d\boldsymbol{\xi}, \\ \rho_0\boldsymbol{u} &= \int f\boldsymbol{\xi}\,d\boldsymbol{\xi} = \int f^{(\mathrm{eq})}\boldsymbol{\xi}\,d\boldsymbol{\xi}, \\ \rho_0 u_i u_j + p\delta_{ij} &= \int f^{(\mathrm{eq})}\xi_i\xi_j\,d\boldsymbol{\xi}. \end{aligned} \tag{38}$$

The Hermite tensorial polynomials are introduced as

$$\omega(\hat{\boldsymbol{\xi}}) = \frac{1}{2\pi}e^{-\hat{\boldsymbol{\xi}}^2/2}, \tag{39}$$

$$H_i^{(n)}(\hat{\boldsymbol{\xi}}) = \frac{(-1)^n}{\omega(\hat{\boldsymbol{\xi}})}\nabla_i^{(n)}\omega(\hat{\boldsymbol{\xi}}), \tag{40}$$

where $\omega(\hat{\boldsymbol{\xi}})$ is the weight function and $\hat{\boldsymbol{\xi}} = \boldsymbol{\xi}/\sqrt{RT}$ is the dimensionless particle velocity [31,32]. The three leading-order Hermite polynomials are expressed as

$$H^{(0)}(\hat{\boldsymbol{\xi}}) = 1, \tag{41a}$$

$$H_i^{(1)}(\hat{\boldsymbol{\xi}}) = \hat{\xi}_i, \tag{41b}$$

$$H_{ij}^{(2)}(\hat{\boldsymbol{\xi}}) = \hat{\xi}_i\hat{\xi}_j - \delta_{ij}. \tag{41c}$$

Then the dimensionless distribution function $\hat{f} = \frac{RT}{\rho_0}f^{(\mathrm{eq})}$ is expanded as

$$\hat{f}(\hat{\boldsymbol{\xi}},\boldsymbol{x},t) = \omega(\hat{\boldsymbol{\xi}})\sum_{n=0}^{\infty}\frac{1}{n!}a_i^{(n)}(\boldsymbol{x},t)H_i^{(n)}(\hat{\boldsymbol{\xi}}), \tag{42}$$

where the expansion coefficient $a_i^{(n)}$ is related to the corresponding moment equations as

$$a_i^{(n)}(\boldsymbol{x},t) = \int \hat{f} H_i^{(n)}(\hat{\boldsymbol{\xi}}) d\hat{\boldsymbol{\xi}} = \frac{1}{\rho_0} \int f^{(\mathrm{eq})} H_i^{(n)}(\hat{\boldsymbol{\xi}}) d\boldsymbol{\xi}. \quad (43)$$

Thus, the equilibrium distribution function with the inclusion of the incompressibility conditions is derived from the modified moments in Eq. (38)

$$f^{(\mathrm{eq})} = \frac{\rho_0}{2\pi RT} \exp\left(-\frac{\boldsymbol{\xi}^2}{2RT}\right)\left[1 + \frac{\boldsymbol{u}\cdot\boldsymbol{\xi}}{RT} + \frac{(\boldsymbol{u}\cdot\boldsymbol{\xi})^2}{2(RT)^2} - \frac{\boldsymbol{u}^2}{2RT} + \left(\frac{p}{\rho_0 RT} - 1\right)\left(\frac{\boldsymbol{\xi}^2}{2RT} - 1\right)\right] \quad (44)$$

and subsequently discretized with the D2Q9 lattice model

$$f_\alpha^{(\mathrm{eq})} = \rho_0 w_\alpha \left\{1 + \frac{\boldsymbol{u}\cdot\boldsymbol{\xi}_\alpha}{RT} + \frac{(\boldsymbol{u}\cdot\boldsymbol{\xi}_\alpha)^2}{2(RT)^2} - \frac{\boldsymbol{u}^2}{2RT} + \left(\frac{p}{\rho_0 RT} - 1\right)\left(\frac{\boldsymbol{\xi}_\alpha^2}{2RT} - 1\right)\right\}. \quad (45)$$

In addition, the discretization of continuous moment equations are also realized as

$$\begin{aligned} \rho_0 &= \sum_\alpha f_\alpha = \sum_\alpha f_\alpha^{(\mathrm{eq})}, \\ \rho_0 u_i &= \sum_\alpha f_\alpha \xi_{\alpha i} = \sum_\alpha f_\alpha^{(\mathrm{eq})} \xi_{\alpha i}, \\ \rho_0 u_i u_j + p\delta_{ij} &= \sum_\alpha f_\alpha^{(\mathrm{eq})} \xi_{\alpha i}\xi_{\alpha j}. \end{aligned} \quad (46)$$

#### 2. *Incompressible method based on the Li et al. model*

A LB equation slightly different that in Ref. [7] is introduced as

$$\begin{aligned} &\hat{f}_\alpha(\boldsymbol{x} + \boldsymbol{\xi}_\alpha\delta t, t+\delta t) - \hat{f}_\alpha(\boldsymbol{x},t) \\ &= -\omega_\alpha\left[\hat{f}_\alpha(\boldsymbol{x},t) - f_\alpha^{(\mathrm{eq})}(\boldsymbol{x},t)\right] + \delta t\left(1 - \frac{\omega_\alpha}{2}\right) S_\alpha \\ &\quad - (\omega_{\boldsymbol{J}} - \omega_f)\frac{3}{8} w_\alpha g_\alpha^{\mathrm{host}} \boldsymbol{\xi}_\alpha \cdot \boldsymbol{J}, \end{aligned} \quad (47)$$

where the last term is added to improve the numerical stability of the present incompressible model with $\omega_f = 2/(2\tau+1)$ being the constant part of $\omega_\alpha$. In particular, the equilibrium distribution functions in Eqs. (7) and (45) can be regarded as a second-order expansion in terms of the first three tensor Hermite polynomials $1, \boldsymbol{\xi}$, and $\boldsymbol{\xi}\boldsymbol{\xi} - \frac{1}{3}I$. With the D2Q9 lattice model, the components of tensor polynomials are composed of the six nine-dimensional lattice vectors

$$\begin{aligned} |1\rangle &= (1,1,1,1,1,1,1,1,1)^T, && (48a)\\ |\xi_{\alpha r}\rangle &= (0,1,0,-1,0,1,-1,-1,1)^T, && (48b)\\ |\xi_{\alpha z}\rangle &= (0,0,1,0,-1,1,1,-1,-1)^T, && (48c)\\ \left|\xi_{\alpha r}^2 - \tfrac{1}{3}\right\rangle &= \tfrac{1}{3}(-1,2,-1,2,-1,2,2,2,2)^T, && (48d)\\ |\xi_{\alpha r}\xi_{\alpha z}\rangle &= (0,0,0,0,0,1,-1,1,-1)^T, && (48e)\\ \left|\xi_{\alpha z}^2 - \tfrac{1}{3}\right\rangle &= \tfrac{1}{3}(-1,-1,2,-1,2,2,2,2,2)^T, && (48f) \end{aligned}$$

which are orthogonal with respect to the weighted inner product $\langle p,q\rangle = \sum_\alpha w_\alpha p_\alpha q_\alpha$, as a direct analogy to the orthogonality of the continuous tensor Hermite polynomials. Furthermore, an $R^9$ orthogonal basis is completed by introducing the ghost vectors $g_\alpha^{\mathrm{host}}$ and $g_\alpha^{\mathrm{host}}\xi_\alpha$,

$$\begin{aligned} \left|g_\alpha^{\mathrm{host}}\right\rangle &= \tfrac{9}{2}\left(|\boldsymbol{\xi}_\alpha|^4 - \tfrac{15}{9}|\boldsymbol{\xi}_\alpha|^2 + \tfrac{2}{9}\right) \\ &= (1,-2,-2,-2,-2,4,4,4,4)^T, && (49a)\\ \left|g_\alpha^{\mathrm{host}}\xi_{\alpha r}\right\rangle &= (0,-2,0,2,0,4,-4,-4,4)^T, && (49b)\\ |g_\alpha^{\mathrm{host}}\xi_{\alpha z}\rangle &= (0,0,-2,0,2,4,4,-4,-4)^T, && (49c) \end{aligned}$$

and the corresponding macroscopic variables, ghost variables, are defined as

$$\begin{aligned} N &= \sum_\alpha \hat{f}_\alpha g_\alpha^{\mathrm{host}}, && (50a)\\ \boldsymbol{J} &= \sum_\alpha \hat{f}_\alpha g_\alpha^{\mathrm{host}} \boldsymbol{\xi}_\alpha, && (50b) \end{aligned}$$

which are directly the high-order moments and have no explicit effect on the evolution of the hydrodynamic variables (i.e., the nonghost variables) [43–46]. With the complete orthogonal basis given in Eqs. (48) and (49), the single relaxation time collision model in Ref. [7] in Eq. (10) with the exclusion of source terms representing the axisymmetric conditions becomes

$$\Omega_\alpha = -\omega_f\left[\hat{f}_\alpha(\boldsymbol{x},t) - f_\alpha^{(\mathrm{eq})}(\boldsymbol{x},t)\right] \quad (51a)$$

and is generalized as (refer to [47] for derivation details)

$$\begin{aligned} \Omega'_\alpha = -w_\alpha\big[&\tfrac{9}{2}s_3\Pi_{rr}^{(\mathrm{neq})}Q_{\alpha rr} + 9s_4\Pi_{rz}^{(\mathrm{neq})}Q_{\alpha rz} \\ &+ \tfrac{9}{2}s_5\Pi_{zz}^{(\mathrm{neq})}Q_{\alpha zz} + g_\alpha^{\mathrm{host}}\left(\tfrac{1}{4}s_6 N + \tfrac{3}{8}s_7 J_r\xi_{\alpha r}\right. \\ &\left.+ \tfrac{3}{8}s_8 J_z\xi_{\alpha z}\right)\big], \end{aligned} \quad (51b)$$

where $\boldsymbol{Q}_\alpha = \boldsymbol{\xi}_\alpha\boldsymbol{\xi}_\alpha - \frac{1}{3}\boldsymbol{I}$ and $\boldsymbol{\Pi}^{(\mathrm{neq})} = \sum_\alpha(\hat{f}_\alpha - f_\alpha^{(\mathrm{eq})})(\boldsymbol{\xi}_\alpha\boldsymbol{\xi}_\alpha - \frac{1}{3}\boldsymbol{I})$ are, respectively, the discrete second-order Hermite polynomial and the relevant nonequilibrium moment and thus the MRT collision model based on the basis in Eqs. (48) and (49) is obtained. The moment components are simply derived from the moment equations of the distribution function and the MRT model would degrade to the BGK model in Eq. (51a) when all the relaxation parameters $s_i$ are equal to $\omega_f$. As discussed by Dellar [44], the coupling between the ghost variables and the hydrodynamic variables is mainly responsible for the numerical instability of the LB simulation. Therefore, in the RLBGK scheme [37,38], both $N$ and $\boldsymbol{J}$ are removed for the purpose of stabilizing the LB method with the prescribed relaxation parameters

$$s_3 = s_4 = s_5 = \omega_f, \quad s_6 = s_7 = s_8 = 1. \quad (52)$$

Thus, the postcollision distribution function $\hat{f}_\alpha^+$ depends only on the hydrodynamic moments as

$$\hat{f}_\alpha^+(\boldsymbol{x},t) = \hat{f}_\alpha^{(\mathrm{eq})}(\boldsymbol{x},t) + w_\alpha\tfrac{9}{2}(1-\omega_f)\boldsymbol{\Pi}^{(\mathrm{neq})} : \boldsymbol{Q}_\alpha, \quad (53)$$

which accords well with the original idea by Ladd [48,49]. In the present model, the last term in Eq. (47) is introduced in accordance with the idea of the RLBGK scheme to suppress

the effect of the ghost variable $\boldsymbol{J}$. Specifically, if the additional relaxation parameter $\omega_{\boldsymbol{J}}$ equals 1, the effect of the ghost variable $\boldsymbol{J}$ is totally removed. Since the variable $\boldsymbol{J}$ is mainly responsible for the coupling with the hydrodynamic variables, the numerical stability of the present method is effectively enhanced by the additional relaxation term and the modified BGK collision operator adopted in Eq. (47) is essentially also a specific case of the general MRT operator in Eq. (51b) with

$$s_3 = s_4 = s_5 = s_6 = \omega_f, \quad s_7 = s_8 = \omega_{\boldsymbol{J}}. \tag{54}$$

The incompressibility conditions are also incorporated into the source terms in Eq. (47) as

$$S_\alpha = S_\alpha^1 + S_\alpha^2, \tag{55a}$$

$$S_\alpha^1 = -\frac{\rho_0 u_r}{r} w_\alpha \left(1 + \frac{\boldsymbol{u}\cdot\boldsymbol{\xi}_\alpha}{RT}\right), \tag{55b}$$

$$S_\alpha^2 = w_\alpha \left[\frac{F_i \xi_{\alpha i}}{RT} + \frac{u_i F_j \xi_{\alpha i}\xi_{\alpha j}}{(RT)^2} - \frac{F_i u_i}{RT}\right],$$

$$F_i = -\left(\frac{2\rho_0 \nu u_r}{r^2} - \frac{\rho_0 u_\theta^2}{r}\right)\delta_{ir}, \tag{55c}$$

which are the direct Hermite expansion pertaining to the moment constraints of the source terms

$$\sum_\alpha S_\alpha^1 = -\frac{\rho_0 u_r}{r}, \quad \sum_\alpha S_\alpha^1 \xi_{\alpha i} = -\frac{\rho_0 u_i u_r}{r}, \tag{56a}$$

$$\sum_\alpha S_\alpha^2 \xi_{\alpha i} = F_i, \quad \sum_\alpha S_\alpha^2 \xi_{\alpha i}\xi_{\alpha j} = F_i u_j + F_j u_i. \tag{56b}$$

Finally, the present incompressible model is completed by the following computing formulas for the macroscopic variables:

$$u_i = \frac{\sum_\alpha \hat{f}_\alpha \xi_{\alpha i} + \frac{\rho_0 u_\theta^2}{2r}\delta_{ir}}{\sum_\alpha \hat{f}_\alpha + (\delta t \rho_0 \nu / r^2)\delta_{ir}}. \tag{57}$$

The application of the present model for axisymmetric convection diffusion equation is similar to the Li *et al.* [7] model by setting the fluid density to be a constant $\rho_0$. In addition, the fluid pressure in the present model is calculated as

$$p = \left(\sum_\alpha \hat{f}_\alpha \xi_{\alpha i}\xi_{\alpha i} - (2\tau + 2)\delta t \rho_0 RT \frac{u_r}{r} - \rho_0 \boldsymbol{u}^2\right)\Big/ 2, \tag{58}$$

which results from the second-order moment equations (see Appendix D for details)

$$\sum_\alpha f_\alpha \xi_{\alpha i}\xi_{\alpha j} = \sum_\alpha \left(f_\alpha^{(\mathrm{eq})} + f_\alpha^{(\mathrm{neq})}\right)\xi_{\alpha i}\xi_{\alpha j}. \tag{59}$$

Here $f_\alpha^{(\mathrm{neq})}$ is the nonequilibrium part of the distribution function and its second-order moment is given by the Chapman-Enskog analysis as

$$\sum_\alpha f_\alpha^{(\mathrm{neq})} \xi_{\alpha i}\xi_{\alpha j} = -\tau \delta t \rho_0 RT \left(\frac{\partial u_i}{\partial x_j} + \frac{\partial u_j}{\partial x_i}\right). \tag{60}$$

### 3. *Incompressible method based on the Zhou model*

A similar incompressible model is also proposed by applying the idea of Zhou [9]. The LB equation in the Zhou [9] model is rewritten as

$$f_\alpha(\boldsymbol{x} + \boldsymbol{\xi}_\alpha \delta t, t + \delta t) - f_\alpha(\boldsymbol{x}, t)$$
$$= -\tau_\alpha \left(f_\alpha - f_\alpha^{(\mathrm{eq})}\right)\big|_{(\boldsymbol{x},t)} - \left(\omega_{\boldsymbol{J}} - \frac{1}{\tau}\right)\frac{3}{8} w_\alpha g_\alpha^{\mathrm{host}} \boldsymbol{\xi}_\alpha \cdot \boldsymbol{J}$$
$$+ w_\alpha \theta \delta t + \frac{w_\alpha}{RT} F_i \xi_{\alpha i} \delta t, \tag{61}$$

where the ghost variable $\boldsymbol{J}$ is directly determined as

$$\boldsymbol{J} = \sum_\alpha f_\alpha g_\alpha^{\mathrm{host}} \boldsymbol{\xi}_\alpha. \tag{62}$$

The source terms are revised in accordance with the incompressibility conditions

$$\theta = -\frac{\rho_0 u_r}{r}\bigg|_{(\boldsymbol{x}+\boldsymbol{\xi}_\alpha \delta t/2, t+\delta t/2)}, \tag{63a}$$

$$F_i = -\left(\frac{\rho_0 u_i u_r}{r} + \frac{2\rho_0 \nu u_r}{r^2}\delta_{ir} - \frac{\rho_0 u_\theta^2}{r}\delta_{ir}\right)\bigg|_{(\boldsymbol{x}+\boldsymbol{\xi}_\alpha \delta t/2, t+\delta t/2)} \tag{63b}$$

Then the computing formula for fluid velocity is obtained as

$$u_i = \sum_\alpha f_\alpha \xi_{\alpha i}/\rho_0, \tag{64}$$

while the fluid pressure is determined from the diagonal part of the second-order moment equations (see Appendix D for detailed deviations)

$$p = \left(\sum_\alpha f_\alpha \xi_{\alpha i}\xi_{\alpha i} - 2\tau \delta t \rho_0 RT \frac{u_r}{r} - \rho_0 \boldsymbol{u}^2\right)\Big/ 2. \tag{65}$$

The present incompressible model can also be extended to solve the axisymmetric convection-diffusion equation by simply prescribing the fluid density involved in Eq. (32) to be $\rho_0$.

To conclude, the incompressible LB models for axisymmetric flows are developed here based on the ideas of two consistent axisymmetric LB models. The present incompressible models retain the advantages of the original models [7,9] in that the framework of the conventional standard LB method is preserved by the present incompressible models and the source terms are simple and contain no velocity gradients. However, the equilibrium distribution functions are reconstructed with the inclusion of the incompressibility conditions by applying the Hermite tensorial polynomials. Furthermore, an additional relaxation parameter pertaining to the ghost variable is introduced to improve the numerical stability of the present models. The Chapman-Enskog analysis in Appendixes A and B demonstrates that the incompressible axisymmetric NS equations (1) are recovered from both proposed incompressible models with truncation terms of second order in Ma, which accords well with the accuracy of the standard LB method when approximating the incompressible NS equations. Furthermore, derivations of the equivalent moment systems under the diffusive scaling [39,41], in Appendix C, demonstrate that the constant density assumption is helpful in reducing the truncation error terms, therefore, the compressibility errors in the Li *et al.* [7] and Zhou [9] models are expected to be decreased by the incompressible models proposed here.

### D. Numerical results

In this section, the proposed incompressible models are numerically validated by some representative tests: the Hagen-Poiseuille flow, the cylindrical cavity flow, the natural convection in an annulus between two coaxial cylinders, and the swirling thermal flows in a cylindrical container. The boundary conditions involved in the following tests, except for the periodic boundary in the axial direction for the Hagen-Poiseuille flow, are implemented by the nonequilibrium extrapolation scheme [50,51], in which the distribution function is first divided into two parts, i.e., the equilibrium part and the remaining nonequilibrium part

$$f_\alpha = f_\alpha^{(\mathrm{eq})} + f_\alpha^{(\mathrm{neq})}. \tag{66}$$

The unknown macroscopic variables at the boundary nodes are determined approximately from the neighboring fluid nodes and then the equilibrium part of the distribution function $f_\alpha^{(\mathrm{eq})}$ is obtained from the definition in Eqs. (7) and (45). In particular, as for the symmetry condition at $r = 0$, the physical boundary constraints are given as (for $r = 0$)

$$\frac{\partial \Phi}{\partial r} = 0 \forall \Phi, \tag{67}$$

with which an arbitrary macroscopic variable $\Phi$ at the symmetry axis is derived from the finite-difference stencil with second-order accuracy

$$\frac{-3\Phi_i^n + 4\Phi_{i+1}^n - \Phi_{i+2}^n}{2\delta x} = \left.\frac{\partial \Phi}{\partial x}\right|_{i,n}. \tag{68}$$

Subsequently, the nonequilibrium part of the distribution function is also extrapolated from the nearest fluid nodes. The resulting boundary scheme agrees well with the overall accuracy of the LB method since the approximations of the macroscopic variables and the extrapolated $f_\alpha^{(\mathrm{neq})}$ are both of second-order accuracy.

#### 1. *Hagen-Poiseuille flow*

The first test case is the Hagen-Poiseuille flow in a cylindrical pipe, with the following analytical solution for axial velocity distribution:

$$u_z(r) = u_0\left(1 - \frac{r^2}{R^2}\right), \tag{69}$$

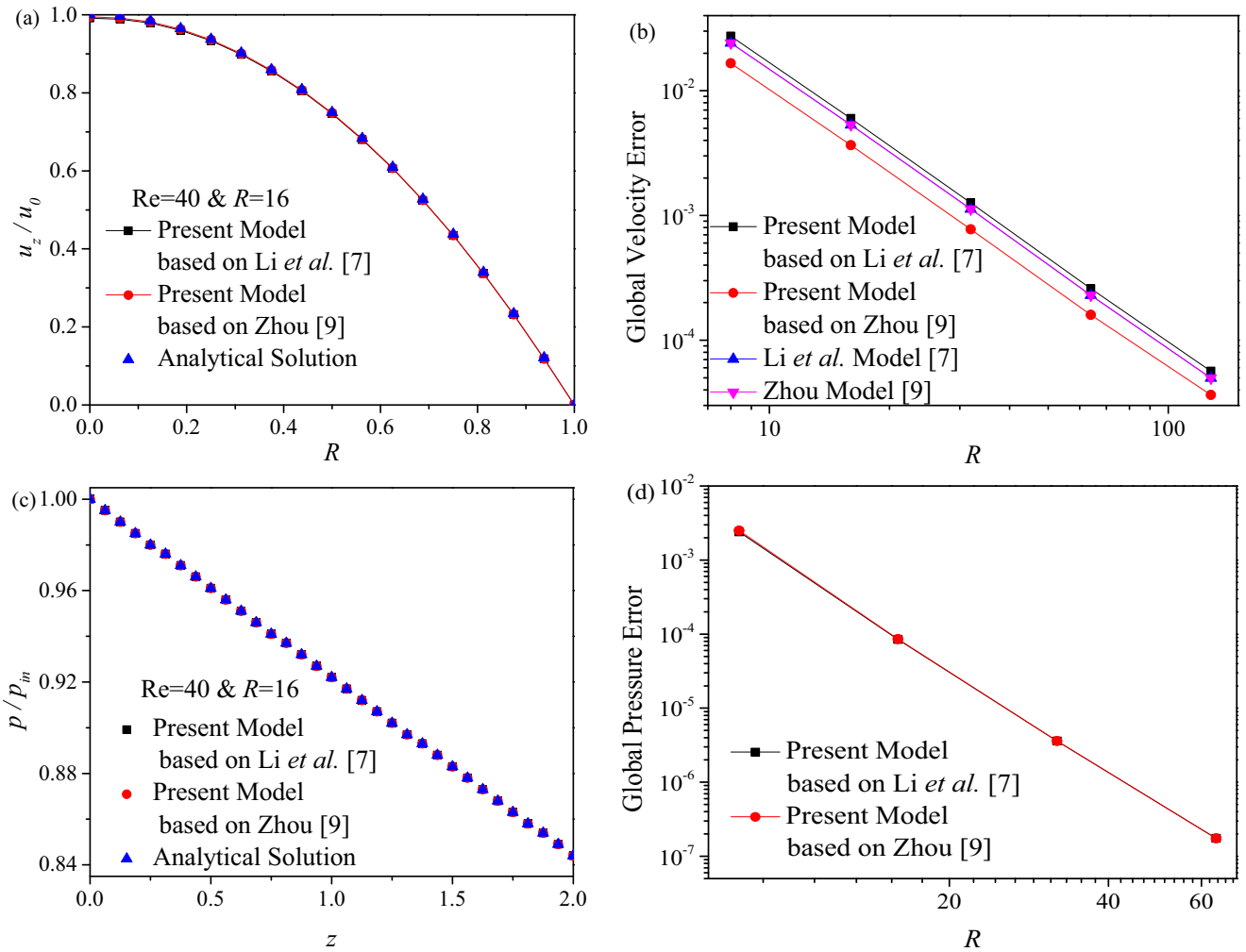


FIG. 1. (a) Axial velocity profile, (b) convergence of the global velocity error with respect to mesh resolution for the Hagen-Poiseuille flow, (c) pressure distribution, and (d) global pressure error convergence.

where $u_0$ is the peak axial velocity at $r = 0$ and is related to the constant driven force $a_z$ by

$$u_0 = a_z R^2/4\nu, \tag{70}$$

where $R$ and $\nu$ are, respectively, the radius of the pipe and the kinematic viscosity. The only dimensionless parameter, the Reynolds number Re, is defined as $\mathrm{Re} = 2Ru_0/\nu$. In addition, the boundary conditions for the remaining boundaries are provided as (for $r = R$)

$$u_r = u_z = 0 \tag{71}$$

and the periodic condition in the $z$ direction is applied for the two ends of the pipe. First, a mesh resolution of $N_z \times N_r = 33 \times 17$, with $N_z$ and $N_r$ representing the number of lattice nodes in the $z$ and $r$ directions, respectively, is adopted for the test case with $\mathrm{Re} = 40$ and $\tau = 0.65$. As shown in Fig. 1(a), the velocity profiles from the proposed models agree with each other and both agree well with the theoretical solutions. Then the convergence rates of the global errors are investigated for the purpose of evaluating the overall accuracy of the proposed models. A definition for the global error is introduced as

$$E(u) = \frac{\left\| u_z - u_z^{\text{analytical}} \right\|_2}{\left\| u_z^{\text{analytical}} \right\|_2}. \tag{72}$$

The global velocity errors pertaining to various mesh resolutions are plotted in Fig. 1(b). It is demonstrated that (i) the global errors from all the LB models investigated converge at the same rate; (ii) the two original models, i.e., those of Li *et al.* [7] and Zhou [9], agree numerically; and (iii) the incompressible model based on Zhou's [9] is more accurate than the two original models [7,9]. Since the radial velocity

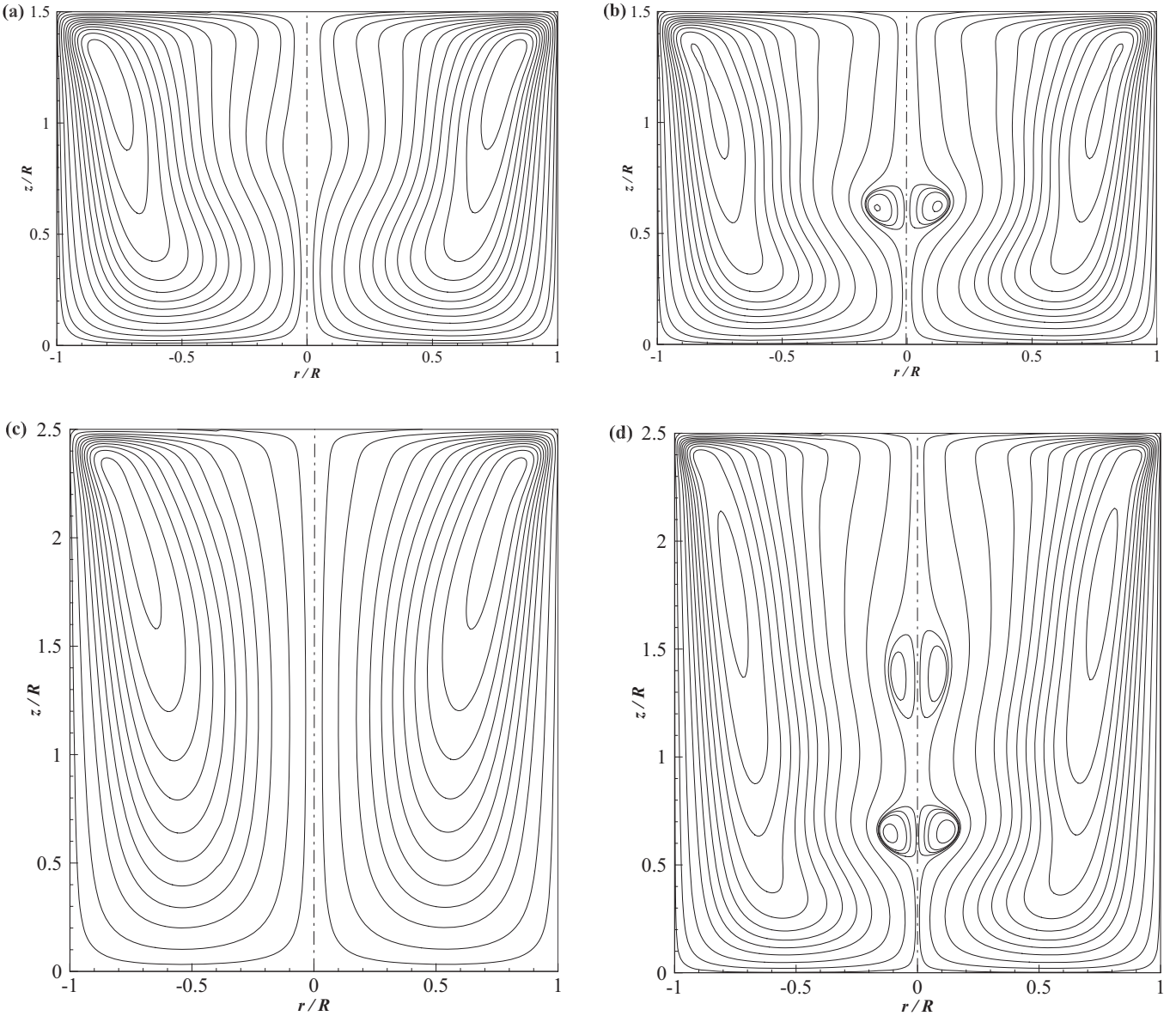


FIG. 2. Flow structure of the cylindrical cavity flow: (a) case A, ($R_A = 1.5$, $\mathrm{Re} = 990$); (b) case B, ($R_A = 1.5$, $\mathrm{Re} = 1290$); (c) case C, ($R_A = 2.5$, $\mathrm{Re} = 1010$); and (d) case D, ($R_A = 2.5$, $\mathrm{Re} = 2200$).

component vanishes and the driving force is constant in the present test case, the source terms are extremely simple. More complicated cases are necessary to further evaluate the accuracy of the proposed models, which are given in the following.

Furthermore, to further validate the accuracy of the pressure formulas of the proposed incompressible axisymmetric models [i.e., in Eqs. (58) and (65)], another test is carried out by replacing the constant driven force $a_z$ with fixed inlet and outlet pressure difference, i.e., $\Delta p = p_{\text{in}} - p_{\text{out}} = a_z L$, where $L$ is the length of the pipe channel. The quantitative pressure distribution obtained from the present incompressible models with a grid resolution of $R = 16$ is given in Fig. 1(c) to compare against the analytical linear pressure distribution. In addition, analogous to the global velocity error definition in Eq. (72), a global pressure error is defined as

$$E(p) = \frac{\|p - p^{\text{analytical}}\|_2}{\|p^{\text{analytical}}\|_2}. \tag{73}$$

The convergence of the global pressure errors at various mesh resolutions is demonstrated in Fig. 1(d). It is concluded from both Figs. 1(c) and 1(d) that pressure can be accurately predicted by the pressure calculations of the present incompressible models.

### 2. *Cylindrical cavity flow*

The second test adopted for the numerical validations is the cylindrical cavity flow, which is driven by rotating the top lid at a constant angular velocity Ω. The geometric configuration of the cylindrical cavity is defined by its height $H$ and radius $R$, which leads to the definition of the aspect ratio $R_A = H/R$. The other dimensionless parameter, which reflects the flow structures, is the Reynolds number $\text{Re} = \Omega R^2/\nu$. In addition to the symmetry condition at $r = 0$, no-slip boundary conditions (i.e., $u_r = u_z = u_\theta = 0$) are imposed on the stagnant bottom and cylindrical surface, and $u_r = u_z = 0$ and $u_\theta = \Omega r$ for the top lid. Since the rotation makes the source terms in the

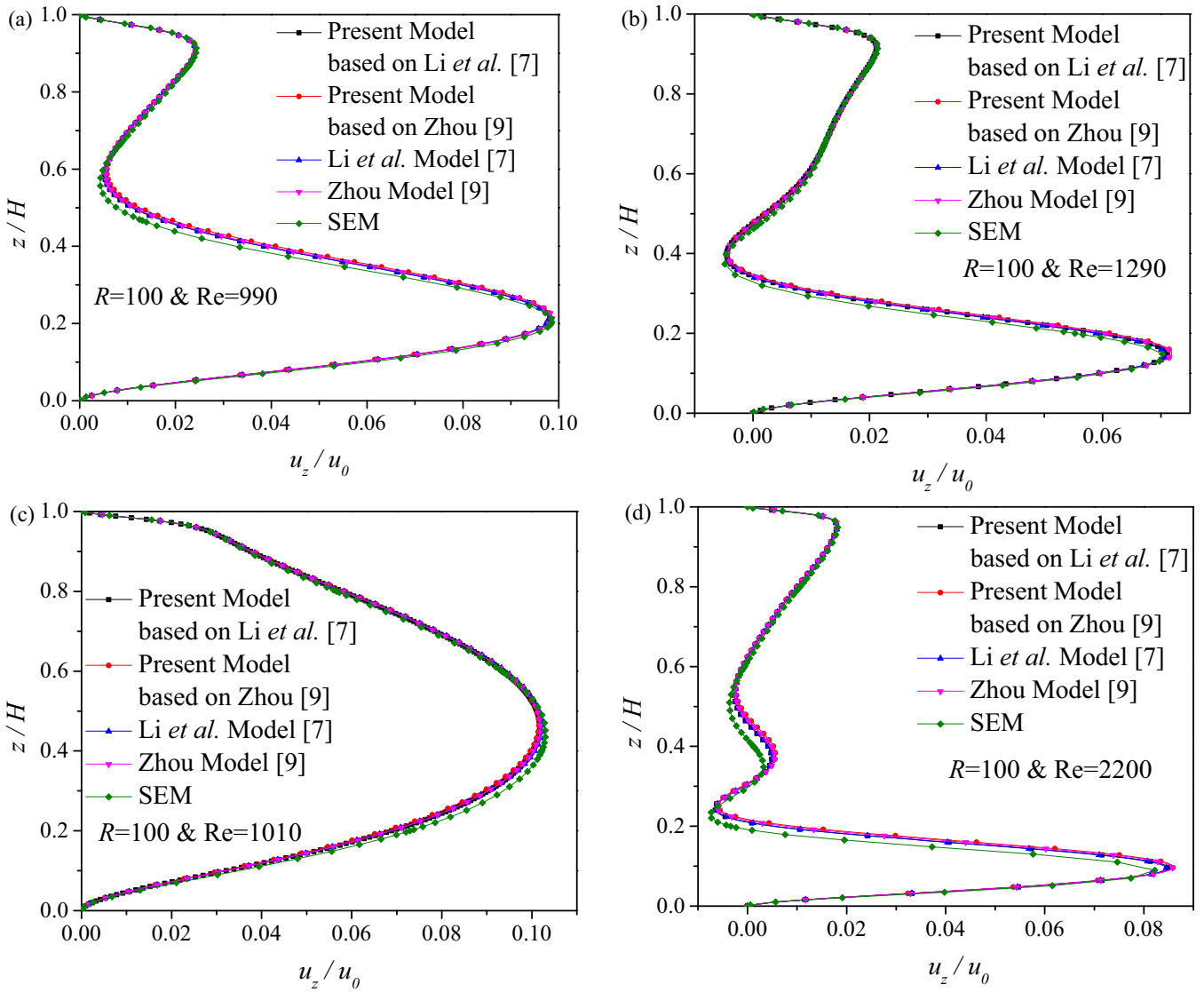


FIG. 3. Axial velocity profiles of the cylindrical cavity flow obtained with an R = 100 lattice: (a) case A, ($R_A = 1.5$, Re = 990); (b) case B, ($R_A = 1.5$, Re = 1290); (c) case C, ($R_A = 2.5$, Re = 1010); and (d) case D, ($R_A = 2.5$, Re = 2200).

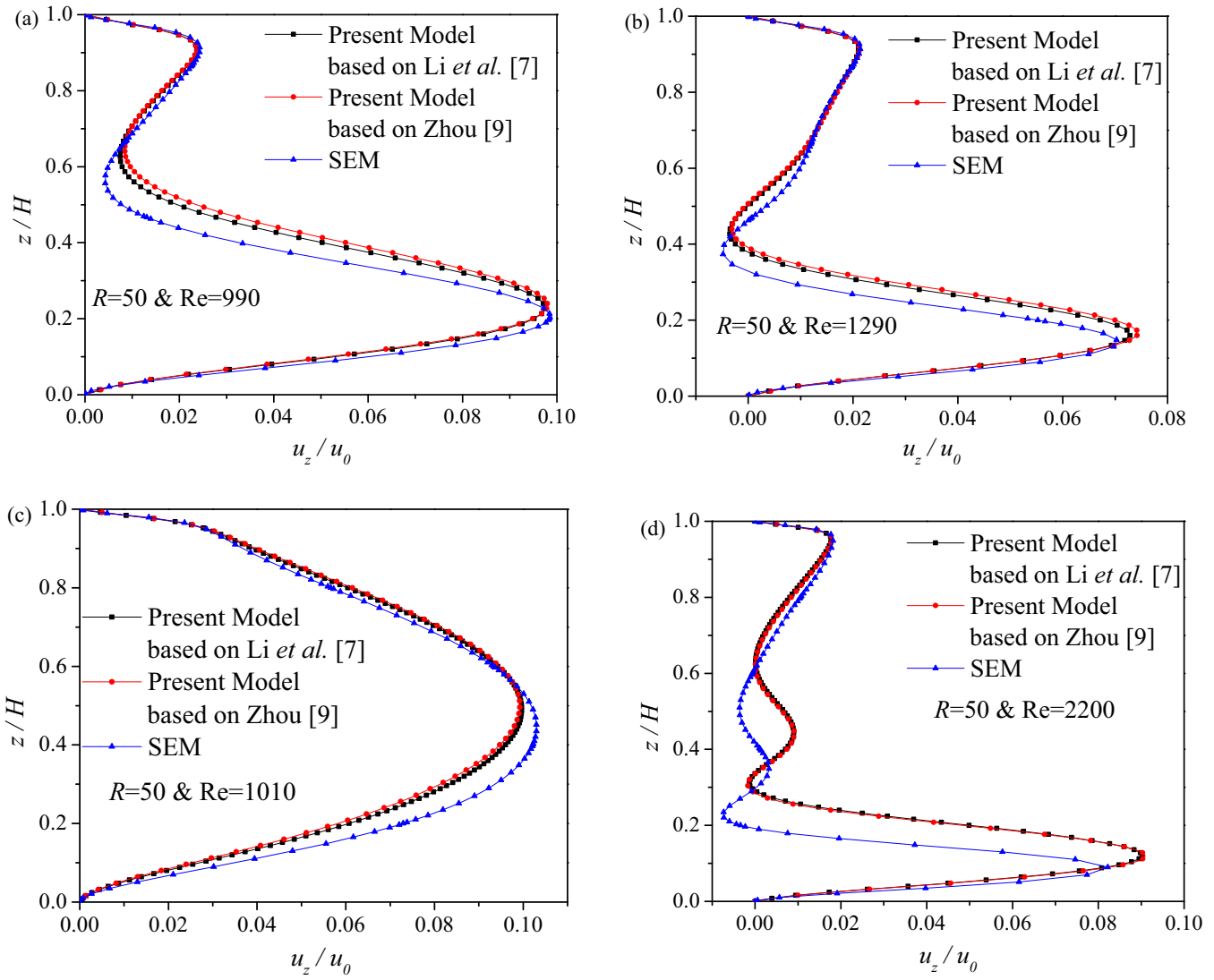


FIG. 4. Axial velocity profiles of the cylindrical cavity flow obtained with an $R = 50$ lattice: (a) case A, ($R_A = 1.5$, Re $= 990$); (b) case B, ($R_A = 1.5$, Re $= 1290$); (c) case C, ($R_A = 2.5$, Re $= 1010$); and (d) case D, ($R_A = 2.5$, Re $= 2200$).

axisymmetric LB model more complicated, the cylindrical cavity flow has been widely used for the evaluation of various axisymmetric LB models [7,9,10,14,52]. In addition, reference solutions from other methods, such as conventional NS solvers [53], the 3D LB method [53], the LB flux solver [52], and even an experimental method [54], are available for comparison with the present test. However, quantitative comparisons suggest that previous published results are not consistent with each other and thus the results from the spectral element method (SEM), which is acknowledged to have high-order accuracy, are introduced as the reference solutions. It should be noted that all the LB simulations of the present test in this work converges to the SEM results when enough mesh resolution is employed.

With the proposed incompressible models, four test cases in terms of ($R_A$,Re) are investigated: A, (1.5, 990); B, (1.5, 1290); C, (2.5, 1010); and D, (2.5, 2200). The steady results for all the cases are obtained with a mesh resolution of

TABLE I. Mass differences caused by the proposed incompressible axisymmetric models in the cylindrical cavity flow test.

| | Present model based on Li *et al.* [7] | | | | Present model based on Zhou [9] | | | |
|---|---|---|---|---|---|---|---|---|
| Grid | Re = 990 | Re = 1290 | Re = 1010 | Re = 2200 | Re = 990 | Re = 1290 | Re = 1010 | Re = 2200 |
| $R = 50$ | $1.47 \times 10^{-7}$ | $1.57 \times 10^{-7}$ | $1.03 \times 10^{-7}$ | $1.60 \times 10^{-7}$ | $2.40 \times 10^{-7}$ | $2.17 \times 10^{-7}$ | $1.77 \times 10^{-7}$ | $1.45 \times 10^{-7}$ |
| $R = 100$ | $2.47 \times 10^{-8}$ | $2.80 \times 10^{-8}$ | $1.68 \times 10^{-8}$ | $9.12 \times 10^{-10}$ | $5.51 \times 10^{-8}$ | $5.35 \times 10^{-8}$ | $3.83 \times 10^{-8}$ | $3.42 \times 10^{-8}$ |

TABLE II. Compressibility errors caused by the Li *et al.* [7] model and its derivative incompressible model.

| | Present model based on Li *et al.* [7] | | | | Li *et al.* [7] | | | |
|---|---|---|---|---|---|---|---|---|
| Grid | Re = 990 | Re = 1290 | Re = 1010 | Re = 2200 | Re = 990 | Re = 1290 | Re = 1010 | Re = 2200 |
| $R = 50$ | $3.09 \times 10^{-4}$ | $3.33 \times 10^{-4}$ | $1.77 \times 10^{-4}$ | $2.22 \times 10^{-4}$ | $3.82 \times 10^{-4}$ | $4.11 \times 10^{-4}$ | $2.26 \times 10^{-4}$ | $2.73 \times 10^{-4}$ |
| $R = 100$ | $1.17 \times 10^{-4}$ | $1.31 \times 10^{-4}$ | $6.82 \times 10^{-5}$ | $1.02 \times 10^{-4}$ | $1.48 \times 10^{-4}$ | $1.67 \times 10^{-4}$ | $8.73 \times 10^{-5}$ | $1.22 \times 10^{-4}$ |

$R = 100$ (i.e., $R$ is divided into 100 lattices with $\delta x$ and $\delta t$ being dimensionless constants equal to 1) and the relevant flow structures are displayed in Fig. 2. In particular, for each plot, the streamlines on the left half are results from the incompressible model based on the Li *et al.* model [7] and the right half is obtained from the incompressible model derived from the Zhou model [9]. The symmetric structures with respect to the vertical centerline in Fig. 2 reflect the consistency between the results from the proposed incompressible models with different origins. Also, the recirculation regions (i.e., the breakdown bubble) along the symmetry axis are not found for lower Re cases, as demonstrated in Figs. 2(a) and 2(c), whereas with the increase of Re one single breakdown bubble appears in case B and two bubbles develop in case D. All the detailed flow configurations shown in Fig. 2 are in line with published results [7,9,10,14,52,53]. Furthermore, quantitative comparisons with the SEM results are performed in terms of the axial velocity component ($u_z/u_0$) profile at the symmetry axis, as exhibited in Fig. 3. It is demonstrated that, under the current mesh resolution of $R = 100$ (i.e., $R$ is divided into 100 lattices), all the results from the LB simulations are consistent with each other and agree well with the reference solutions, which affirms the reliability of the proposed models. Moreover, further comparisons of the accuracy of the proposed incompressible models are carried out with a lower mesh resolution of $R = 50$ (i.e., $R$ is divided into 50 lattices), as illustrated in Fig. 4. Figure 4 shows that results from the incompressible model based the Li *et al.* model [7] are slightly more accurate in terms of better agreement with the SEM for the first two test cases, which may be a direct consequence of the simplified implementation of the source terms in Ref. [9]. Specifically, for the Zhou model [9], the discrete lattice effects cannot be removed completely by the semi-implicit centered scheme in Eq. (29b) and the expressions of the force term are incomplete in comparison with those in Ref. [7] [i.e., Eq. (55c)].

With the present test case, the mass conservation of the proposed incompressible models, i.e., the consistency with the incompressibility conditions, is also investigated. The mass difference is introduced to evaluate the difference between the fluid density in the numerical simulations and the assumed constant density $\rho_0 = 1$. An average fluid density $\bar{\rho}$ is defined as

$$\bar{\rho} = \frac{\sum_{i,j} |M_0(i,j)|}{N_r N_z}, \tag{74}$$

where $M_0 = \sum_\alpha f_\alpha$ is the fluid density obtained from numerical simulations and the mass difference is determined as $\Delta\rho = \bar{\rho} - 1$. The mass differences pertaining to all the test cases are provided in Table I, which shows that, even for the lower mesh resolution, the mass differences from the two incompressible models are less than $2.5 \times 10^{-7}$, which is far less than the global errors given in Fig. 1(b). Moreover, the mass differences from the proposed model based on that of Li *et al.* [7] are generally less than those in the incompressible model derived from the Zhou model [9].

The compressibility error, which can also be used to gauge the accuracy of the models, is defined as

$$E^{\text{compress}} = \frac{\sum_{i,j} \left| \frac{\partial(ru_r)}{\partial r} + \frac{\partial(ru_z)}{\partial z} \right|}{N_r N_z}. \tag{75}$$

Tables II and III present the compressibility errors associated with the incompressible models based on those of Li *et al.* [7] and Zhou [9], respectively. The compressibility errors caused by the Li *et al.* [7] model and the Zhou [9] model are effectively reduced by the respective incompressible models. Quantitatively, the compressibility errors by the original models are approximately 20% larger than the corresponding incompressible models. Therefore, by comparing either the mass difference or compressibility error, incompressibility conditions are consistently more accurately satisfied by the proposed incompressible models.

Furthermore, comparisons of the numerical stability of the proposed incompressible axisymmetric models, in the absence and presence of the additional relaxation term, are given in Table IV. It is demonstrated that the incompressible models with the BGK collision operator (i.e., $\omega_J = \omega_f$) suffer from poor numerical stability and convergent results cannot be obtained for Re $> 400$ at a mesh resolution of $R = 100$. However, the additional relaxation term makes the proposed models more widely applicable by significantly improving the numerical stability. In particular, with $\omega_J = 1$, the effects

TABLE III. Compressibility errors caused by the Zhou [9] model and its derivative incompressible model. Blank entry signifies not convergent.

| | Present model based on Zhou [9] | | | | Zhou [9] | | | |
|---|---|---|---|---|---|---|---|---|
| Grid | Re = 990 | Re = 1290 | Re = 1010 | Re = 2200 | Re = 990 | Re = 1290 | Re = 1010 | Re = 2200 |
| $R = 50$ | $3.22 \times 10^{-4}$ | $3.45 \times 10^{-4}$ | $1.86 \times 10^{-4}$ | $2.21 \times 10^{-4}$ | $3.96 \times 10^{-4}$ | $4.22 \times 10^{-4}$ | $2.39 \times 10^{-4}$ | |
| $R = 100$ | $1.24 \times 10^{-4}$ | $1.38 \times 10^{-4}$ | $7.28 \times 10^{-5}$ | $9.55 \times 10^{-5}$ | $1.45 \times 10^{-4}$ | $1.62 \times 10^{-4}$ | $8.49 \times 10^{-5}$ | $1.40 \times 10^{-4}$ |

TABLE IV. Maximum Re of the convergent simulations based on the incompressible axisymmetric LB model.

| | Incompressible model based on the Li *et al.* [7] model | | | Incompressible model based on the Zhou [9] model | |
|---|---|---|---|---|---|
| Parameters | BGK ($\omega_J = \omega_f$) | $\omega_J = 1.0$ | $\omega_J = 0.9$ | BGK ($\omega_J = \omega_f$) | $\omega_J = 1.0$ |
| $R = 100, R_A = 1.5$ | 400 | 2300 | 2700 | 400 | 2800 |
| $R = 100, R_A = 2.5$ | 400 | 2000 | 2300 | 400 | 2800 |

of the ghost variable $\boldsymbol{J}$ are completely removed and the incompressible axisymmetric model based on the Zhou [9] model can provide convergent results up to $Re = 2800$ at the same grid resolution. Moreover, Table IV indicates that further decreasing the additional relaxation parameter $\omega_J$ (note that $0 < \omega_J < 2$) from 1.0 to 0.9 increases the Re range over which the incompressible axisymmetric model based on the Li *et al.* [7] model remains numerically stable.

### 3. *Natural convection in an annulus between two coaxial vertical cylinders*

Two more thermal tests are investigated to further verify the proposed incompressible LB models. In particular, the effect of the temperature distribution on the velocity fields is considered by invoking the Boussinesq approximation, which leads to an additional external force term related to the temperature differences

$$\rho a_z = -\rho \boldsymbol{g} \beta (T - T_m). \tag{76}$$

Here $\boldsymbol{g}$ and $\beta$ are the gravitational acceleration and thermal-expansion coefficient, respectively, $T - T_m$ denotes the temperature difference, and $T_m$ is the adopted reference temperature.

Here the natural convection in an annulus between two coaxial vertical cylinders is considered. The geometry of the annulus is such that the radii for the inner and outer cylinders are $R_i$ and $R_o$, respectively, and $H$ is the height of the annulus. The relationship between these geometric dimensions is applied $R_o/R_i = H/(R_o - R_i) = 2$. As for the

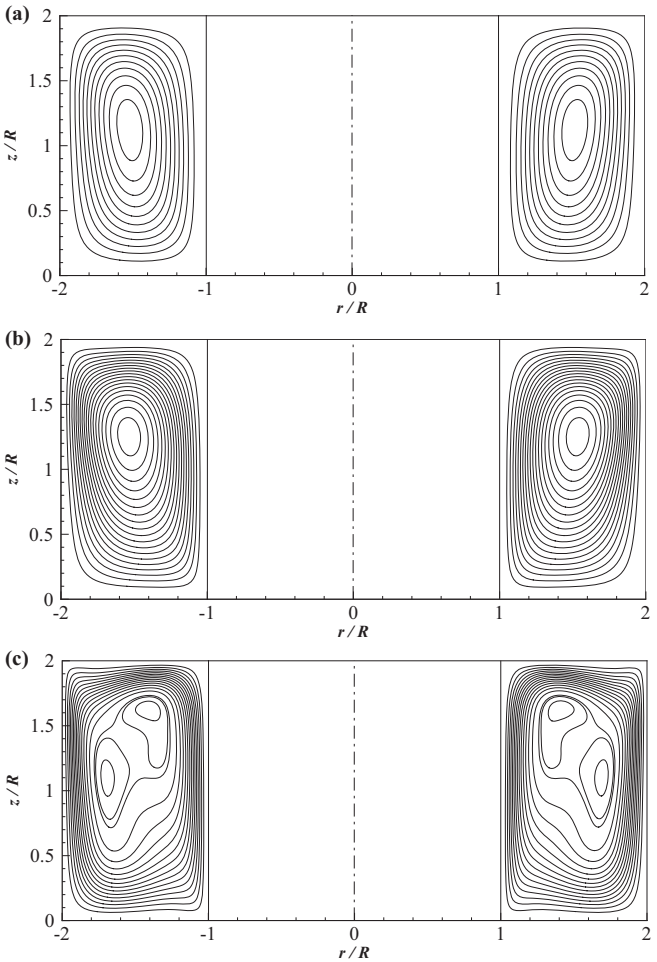


FIG. 5. Streamlines for the natural convection in an annulus at Pr = 0.7 and (a) Ra = $10^3$, (b) Ra = $10^4$, and (c) Ra = $10^5$.

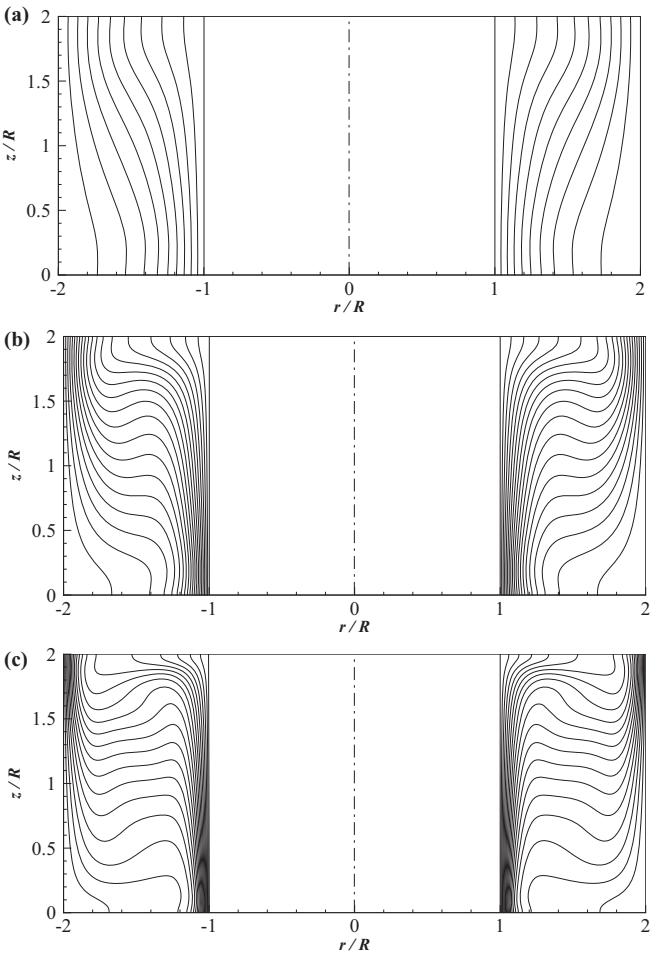


FIG. 6. Isotherms for the natural convection in an annulus at Pr = 0.7 and (a) Ra = $10^3$, (b) Ra = $10^4$, and (c) Ra = $10^5$.

TABLE V. Average Nusselt numbers for the natural convection in a cylindrical annulus. Blank entry signifies not available.

| | LB simulations | | | | Reference results | |
|---|---|---|---|---|---|---|
| Ra | Present model based on Li *et al.* [7] | Present model based Zhou [9] | Li *et al.* [7] | Zhou [9] | Ref. [29] | Ref. [55] |
| $10^3$ | 1.692 | 1.692 | 1.692 | 1.692 | 1.692 | |
| $10^4$ | 3.217 | 3.218 | 3.213 | 3.218 | 3.215 | 3.163 |
| $10^5$ | 5.781 | 5.789 | 5.756 | 5.785 | 5.787 | 5.882 |

boundary conditions, no-slip conditions are applied on all four walls for the velocity field and constant temperatures of $T_i$ and $T_o$ ($T_i > T_o$) are fixed at the inner and outer cylindrical surfaces, respectively, while the top and bottom walls are insulated (i.e., $\partial T/\partial z = 0$). In addition, the reference temperature in Eq. (76) is set at $T_m = (T_i + T_o)/2$. The flow structure depends on two dimensionless parameters, namely, the Prandtl number $\mathrm{Pr} = \nu/\alpha$ and the Rayleigh number $\mathrm{Ra} = g\beta(T_i - T_o)(R_o - R_i)^3/\alpha\nu$. In this work, results for the test cases with a constant $\mathrm{Pr} = 0.7$ and $\mathrm{Ra} = 10^3$, $10^4$, and $10^5$ are obtained from the two proposed incompressible models with a mesh resolution of $R_o - R_i = 100$. Flow structures and temperature distributions for the test cases are demonstrated, respectively, in Figs. 5 and 6. Similar to Fig. 2, the left half and right half present the results from the proposed model based, respectively, on the Li *et al.* and Zhou models [7,9]. The symmetric distribution of the streamlines and the isotherms with respect to the vertical centerline (i.e., the symmetry axis) reflects the consistency of the two proposed incompressible models. Moreover, the detailed flow structures from the present models agree well with the published results [29] in that, with the increase of the Rayleigh number Ra, the flow structures become more complicated and the temperature distributions are more confined to the region near the cylindrical surfaces. The above phenomena can be attributed to the enhanced convection as a result of a larger driven force associated with the increased Ra.

The surface-averaged Nusselt numbers on the cylindrical wall is also employed for quantitative comparisons

$$\mathrm{Nu}_i = -\frac{R_i}{H(T_i - T_o)}\int_0^H \left.\frac{\partial T}{\partial r}\right|_i dz, \tag{77a}$$

$$\mathrm{Nu}_o = -\frac{R_o}{H(T_i - T_o)}\int_0^H \left.\frac{\partial T}{\partial r}\right|_o dz. \tag{77b}$$

The average Nusselt numbers $\mathrm{Nu} = (\mathrm{Nu}_i + \mathrm{Nu}_o)/2$ for the test cases are tabulated in Table V. The quantitative parameters from the two proposed models exactly agree with each other and are consistent with their respective original models [7,9] and reference results based on the Zhou model with the MRT collision operator [29] and the direct NS solutions [55], which again demonstrates the reliability and accuracy of the present incompressible models.

#### *4. Swirling thermal flows in a cylindrical cavity*

The thermal rotating flow in a cylindrical cavity under constant temperature difference is simulated with the proposed incompressible models. The aspect ratio of the cavity $H/R$ is set at 1, where $H$ and $R$ are, respectively, the height

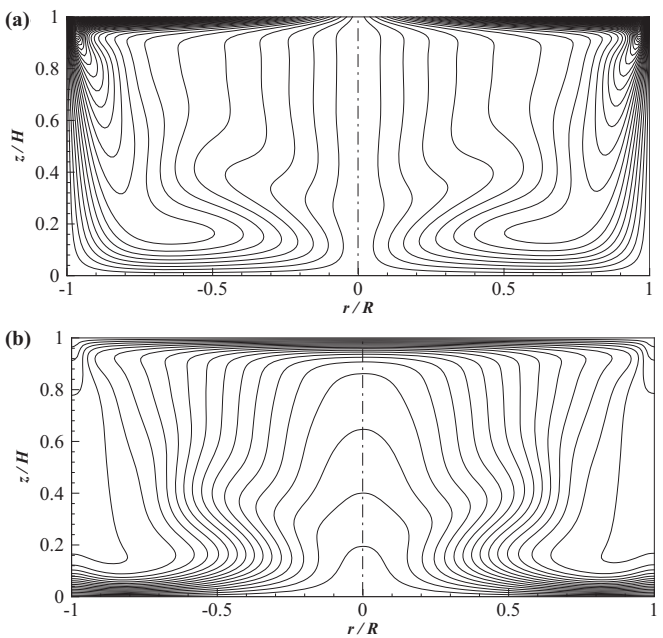


FIG. 7. (a) Azimuthal velocity contours and (b) isotherms for the case of $\mathrm{Ri} = 0$.

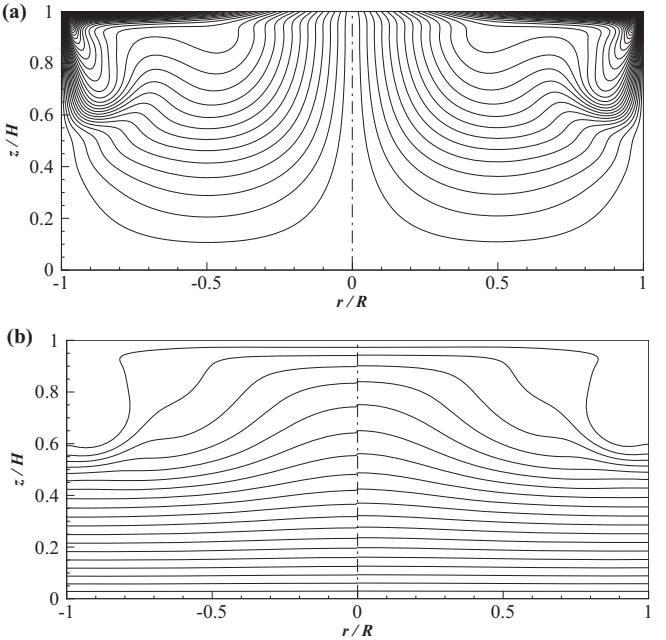


FIG. 8. (a) Azimuthal velocity contours and (b) isotherms for the case of $\mathrm{Ri} = 1$.

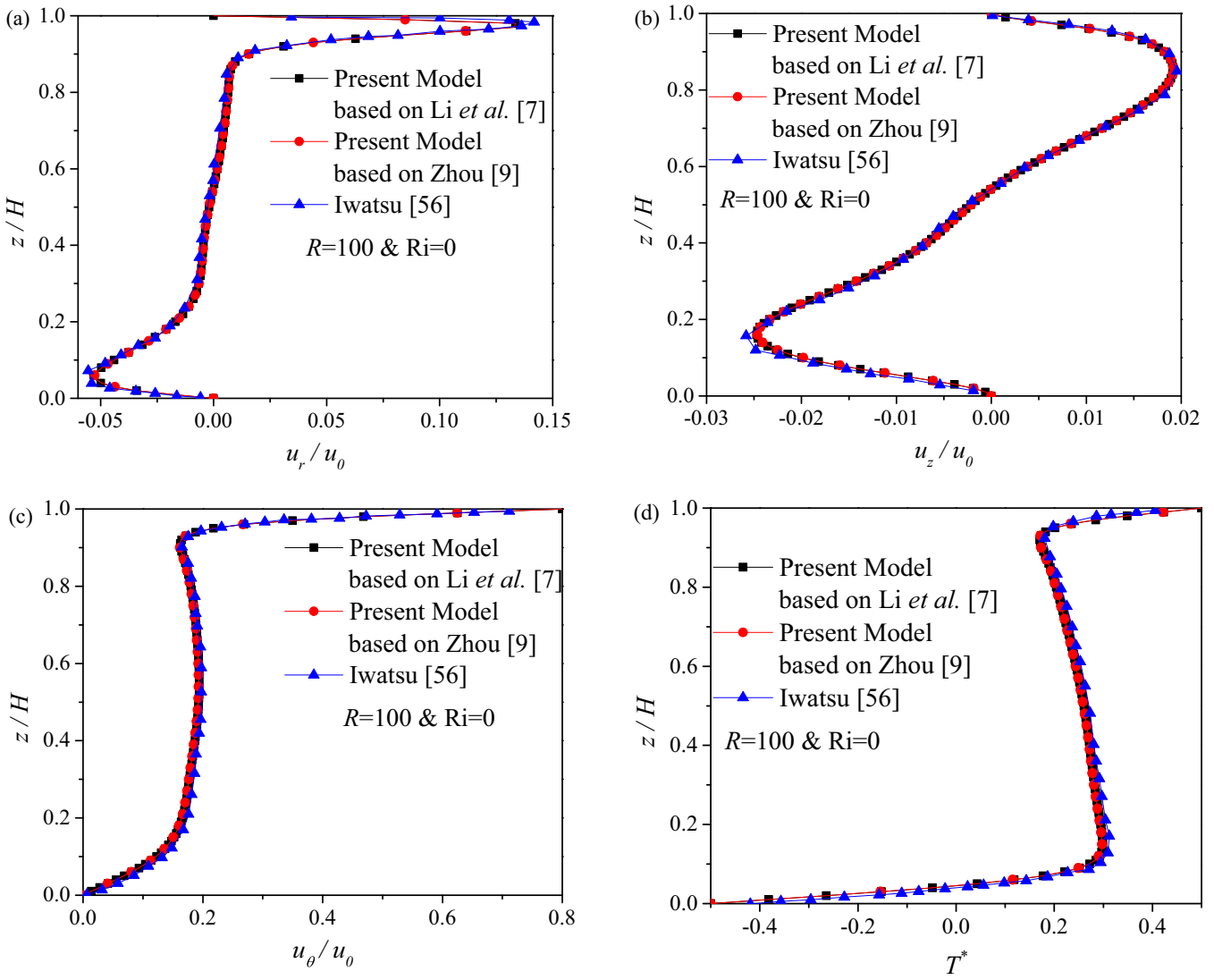


FIG. 9. Profiles of velocity components (a) $u_r/u_0$, (b) $u_z/u_0$, (c) $u_\theta/u_0$, and (d) dimensionless temperature $T^*$ at $r/R = 0.8$ for the case of $\mathrm{Ri} = 0$.

and radius of the cylindrical cavity. The top lid rotates with a constant angular velocity $\Omega$ and the rest of the solid walls are stationary. In addition, constant temperatures of $T_h$ and $T_c$ ($T_h > T_c$) are fixed at the top and bottom walls, respectively, while the vertical cylindrical wall is insulated (i.e., $\partial T/\partial r = 0$). Dimensionless parameters involved in the present test are defined as $\mathrm{Pr} = \nu/\alpha$, $\mathrm{Re} = \Omega R^2/\nu$, and the Richardson number $\mathrm{Ri} = g\beta(T_h - T_c)/R\Omega^2$. Test cases for constant $\mathrm{Pr} = 1.0$ and $\mathrm{Re} = 2000$, and $\mathrm{Ri} = 0$ and 1 are, respectively, considered with mesh resolutions of $R = 100$ and $R = 150$.

Contours for the azimuthal velocity and the isotherms are demonstrated for $\mathrm{Ri} = 0$ (Fig. 7) and $\mathrm{Ri} = 1$ (Fig. 8). The effect of the enhanced buoyancy force when Ri switches from 0 to 1 is such that the distribution of the azimuthal velocity becomes more confined in the vicinity of the top lid [Fig. 8(a)] and the isotherms in the lower half of the cavity become more horizontal [Fig. 8(b)]. The present distributions of the azimuthal velocity and temperature are consistent with the published results [29,56]. Moreover, the velocity components (namely, $u_r/u_0$, $u_z/u_0$, and $u_\theta/u_0$) and the dimensionless temperature $T^*$ profiles at $r = 0.8R$ are given for the cases of $\mathrm{Ri} = 0$ and 1, respectively in Figs. 9 and 10. The dimensionless temperature is defined as $T^* = (T - T_m)/(T_h - T_c)$, whereby $T_m = (T_h + T_c)/2$. All the quantitative results from the LB simulations with the proposed incompressible models agree well with the reference solutions [56]. In addition, for the $\mathrm{Ri} = 1$ case shown in Fig. 10, approximate linear distributions of all the macroscopic variables at the lower half of the cavity are demonstrated, which is consistent with the flow patterns given in Fig. 8.

## III. CONCLUSION

In this work, two incompressible LB models for axisymmetric flows were proposed based on two efficient top-down axisymmetric models, namely, the Li *et al.* [7] and Zhou [9] models. The proposed models are consistent with the basic framework of the conventional LB method and retain the advantages in the existing models [7,9] in that the source terms

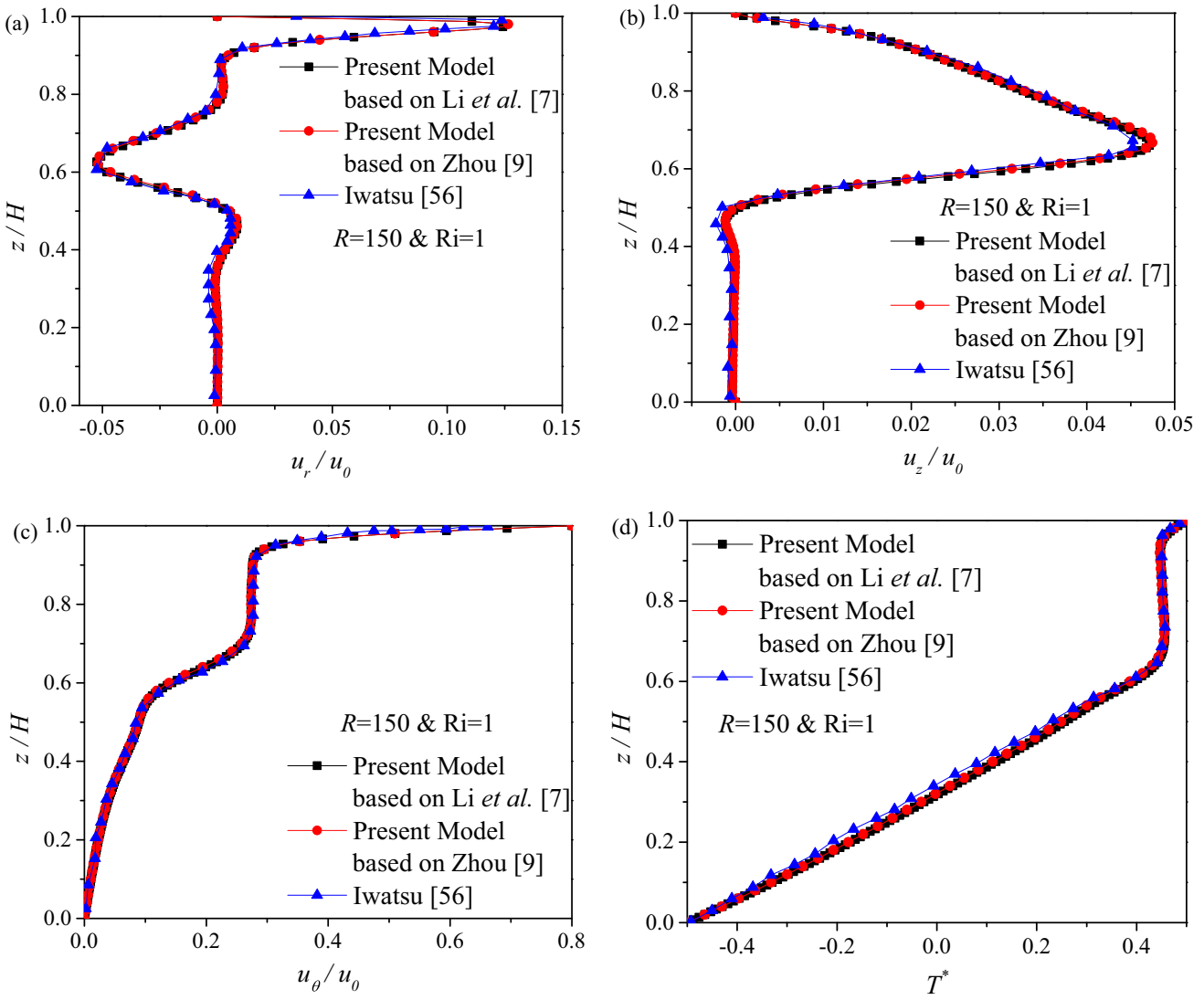


FIG. 10. Profiles of velocity components (a) $u_r/u_0$, (b) $u_z/u_0$, (c) $u_\theta/u_0$, and (d) dimensionless temperature $T^*$ at $r/R = 0.8$ for the case of Ri = 1.

are simple and contain no gradient calculations. Specifically, the incompressibility conditions were introduced by modifying the moment equations of the original models with the assumption of a constant fluid density. The expressions of the equilibrium distribution function and the source terms, as well as the computing formulas of the macroscopic variables, were then derived from the modified moments. In particular, the fluid pressure was determined by the second-order moment of the general distribution function, as derived in Appendix D. In addition, an extra relaxation term was added to reduce the effect of the ghost variables, thereby the numerical stability was efficiently improved.

It was demonstrated from the Chapman-Enskog analysis that the proposed incompressible axisymmetric LB models approximate the standard NS equations for incompressible flows with the same accuracy as their respective original models. Moreover, the equivalent moment system in the diffusive scaling, proposed by Junk [39], further indicates that the constant density assumption in the present models is definitely helpful in reducing the compressibility errors, which was also verified in the tests on practical systems. Furthermore, the overall accuracy and the applicability of the present incompressible models were demonstrated by the well-acknowledged numerical tests since excellent agreement with the reference solutions were obtained. Therefore, both models developed here were shown to be effective for describing incompressible axisymmetric flows.

## ACKNOWLEDGMENTS

We are grateful for financial support from the National Research Foundation, Prime Minister's Office, Singapore under its Campus for Research Excellence and Technological Enterprise program. This work was also financially supported by the National Natural Science Foundation of China (Grant No. 11572062) and the Program for Changjiang Scholars and Innovative Research Team in University (Grant No. IRT13043).

## APPENDIX A

The Chapman-Enskog expansion adopted in previous work [7–9,28] is introduced as

$$\varepsilon = \delta t, \quad f_\alpha = f_\alpha^{(0)} + \varepsilon f_\alpha^{(1)} + \varepsilon^2 f_\alpha^{(2)}, \quad \frac{\partial}{\partial t} = \frac{\partial}{\partial t_0} + \varepsilon \frac{\partial}{\partial t_1}, \tag{A1}$$

with $\varepsilon = \delta t$ being the expansion parameters. In Ref. [7], the source term is also expanded as

$$S_\alpha = S_\alpha^{(0)} + \varepsilon S_\alpha^{(1)}, \quad S_\alpha^{(0)} = -\frac{u_r}{r} f_\alpha^{(\mathrm{eq})}, \quad S_\alpha^{(1)} = -\frac{2\tau u_r(\xi_{\alpha r} - u_r)}{r^2} f_\alpha^{(\mathrm{eq})}. \tag{A2}$$

Then the Taylor expansion of Eq. (5) is obtained as

$$\begin{aligned}\delta t\left(\frac{\partial}{\partial t} + \xi_{\alpha i}\frac{\partial}{\partial x_i}\right) f_\alpha + \frac{\delta t^2}{2}\left(\frac{\partial}{\partial t} + \xi_{\alpha i}\frac{\partial}{\partial x_i}\right)^2 f_\alpha = -\frac{1}{\tau}\left(f_\alpha - f_\alpha^{(\mathrm{eq})}\right) - \frac{\delta t \xi_{\alpha r}}{r}\left(f_\alpha - f_\alpha^{(\mathrm{eq})}\right) - \frac{\delta t}{2\tau}\left(\frac{\partial}{\partial t} + \xi_{\alpha i}\frac{\partial}{\partial x_i}\right) \\ \times \left(f_\alpha - f_\alpha^{(\mathrm{eq})}\right) + \delta t S_\alpha + \frac{\delta t^2}{2}\left(\frac{\partial}{\partial t} + \xi_{\alpha i}\frac{\partial}{\partial x_i}\right) S_\alpha.\end{aligned} \tag{A3}$$

Substituting the expansions in Eqs. (A1) and (A2) into Eq. (A3) we have, for $\varepsilon^0$, $\varepsilon^1$, and $\varepsilon^2$, respectively,

$$f_\alpha^{(0)} = f_\alpha^{(\mathrm{eq})}, \tag{A4a}$$

$$\left(\frac{\partial}{\partial t_0} + \xi_{\alpha i}\frac{\partial}{\partial x_i}\right) f_\alpha^{(0)} = -\frac{1}{\tau} f_\alpha^{(1)} + S_\alpha^{(0)}, \tag{A4b}$$

$$\frac{\partial}{\partial t_1} f_\alpha^{(0)} + \left(\frac{\partial}{\partial t_0} + \xi_{\alpha i}\frac{\partial}{\partial x_i}\right) f_\alpha^{(1)} + \frac{1}{\tau} f_\alpha^{(2)} = S_\alpha^{(1)} - \frac{\xi_{\alpha r}}{r} f_\alpha^{(1)}. \tag{A4c}$$

The leading-order moments of Eq. (A4b) are obtained as

$$\frac{\partial}{\partial t_0}\sum_\alpha f_\alpha^{(0)} + \frac{\partial}{\partial x_i}\sum_\alpha f_\alpha^{(0)}\xi_{\alpha i} = \sum_\alpha S_\alpha^{(0)}, \tag{A5a}$$

$$\frac{\partial}{\partial t_0}\sum_\alpha f_\alpha^{(0)}\xi_{\alpha i} + \frac{\partial}{\partial x_j}\sum_\alpha f_\alpha^{(0)}\xi_{\alpha i}\xi_{\alpha j} = \sum_\alpha S_\alpha^{(0)}\xi_{\alpha i}, \tag{A5b}$$

$$\frac{\partial}{\partial t_0}\sum_\alpha f_\alpha^{(0)}\xi_{\alpha i}\xi_{\alpha j} + \frac{\partial}{\partial x_l}\sum_\alpha f_\alpha^{(0)}\xi_{\alpha i}\xi_{\alpha j}\xi_{\alpha l} = -\frac{1}{\tau}\sum_\alpha f_\alpha^{(1)}\xi_{\alpha i}\xi_{\alpha j} + \sum_\alpha S_\alpha^{(0)}\xi_{\alpha i}\xi_{\alpha j} \tag{A5c}$$

and the moments of Eq. (A4c) are

$$\frac{\partial}{\partial t_1}\sum_\alpha f_\alpha^{(0)} = 0, \tag{A6a}$$

$$\frac{\partial}{\partial t_1}\sum_\alpha f_\alpha^{(0)}\xi_{\alpha i} + \frac{\partial}{\partial x_j}\sum_\alpha f_\alpha^{(1)}\xi_{\alpha i}\xi_{\alpha j} = \sum_\alpha S_\alpha^{(1)}\xi_{\alpha i} - \frac{1}{r}\sum_\alpha f_\alpha^{(1)}\xi_{\alpha i}\xi_{\alpha r}. \tag{A6b}$$

Substituting the moment equations prescribed in Eq. (12) into Eq. (A5), we obtain

$$\frac{\partial}{\partial t_0}\rho + \frac{\partial}{\partial x_i}(\rho u_i) = -\frac{\rho u_r}{r}, \tag{A7a}$$

$$\frac{\partial}{\partial t_0}(\rho u_i) + \frac{\partial}{\partial x_j}(\rho u_i u_j + p\delta_{ij}) = -\frac{\rho u_i u_r}{r}, \tag{A7b}$$

$$\frac{\partial}{\partial t_0}(\rho u_i u_j + p\delta_{ij}) + \frac{\partial}{\partial x_l}[\rho RT(u_i\delta_{jl} + u_j\delta_{il} + u_l\delta_{ij})] = -\frac{1}{\tau}\sum_\alpha f_\alpha^{(1)}\xi_{\alpha i}\xi_{\alpha j} - \frac{u_r}{r}(\rho u_i u_j + p\delta_{ij}), \tag{A7c}$$

which leads to

$$\sum_\alpha f_\alpha^{(1)}\xi_{\alpha i}\xi_{\alpha j} = -\tau\left[\rho RT\left(\frac{\partial u_i}{\partial x_j} + \frac{\partial u_j}{\partial x_i}\right) - \frac{\partial(\rho u_i u_j u_k)}{x_k}\right] = -\tau\rho RT\left(\frac{\partial u_i}{\partial x_j} + \frac{\partial u_j}{\partial x_i}\right) + O(\mathrm{Ma}^3). \tag{A8}$$

Then Eqs. (A6a) and (A6b) are rewritten as

$$\frac{\partial}{\partial t_1}\rho = 0, \tag{A9a}$$

$$\frac{\partial}{\partial t_1}(\rho u_i) - \frac{\partial}{\partial x_j}\left[\tau\rho RT\left(\frac{\partial u_i}{\partial x_j} + \frac{\partial u_j}{\partial x_i}\right)\right] = -\frac{2\tau\rho RTu_r}{r^2}\delta_{ir} + \frac{\tau}{r}\rho RT\left(\frac{\partial u_i}{\partial r} + \frac{\partial u_r}{\partial x_i}\right). \tag{A9b}$$

Combining Eqs. (A7a) and (A7b) with Eqs. (A9a) and (A9b), respectively, the macroscopic equations pertaining to the Li *et al.* [7] model are obtained as

$$\frac{\partial}{\partial t}\rho + \frac{\partial}{\partial x_i}(\rho u_i) = -\frac{\rho u_r}{r}, \tag{A10a}$$

$$\frac{\partial}{\partial t}(\rho u_i) + \frac{\partial}{\partial x_j}(\rho u_i u_j + p\delta_{ij}) + \frac{\rho u_i u_r}{r} = \frac{\partial}{\partial x_j}\left[\mu\left(\frac{\partial u_i}{\partial x_j} + \frac{\partial u_j}{\partial x_i}\right)\right] + \frac{\mu}{r}\left(\frac{\partial u_i}{\partial r} + \frac{\partial u_r}{\partial x_i}\right) - \frac{2\mu u_r}{r^2}\delta_{ir} + O(\mathrm{Ma}^3), \tag{A10b}$$

with the dynamic viscosity $\mu = \tau\rho RT\delta t$.

Similarly, applying the modified moment equations (46) to Eqs. (A5) and (A6), the moments of the expanded equations for the relevant incompressible model are derived as

$$\frac{\partial}{\partial t_0}\rho_0 + \frac{\partial}{\partial x_i}(\rho_0 u_i) = -\frac{\rho_0 u_r}{r}, \tag{A11a}$$

$$\frac{\partial}{\partial t_0}(\rho_0 u_i) + \frac{\partial}{\partial x_j}(\rho_0 u_i u_j + p\delta_{ij}) = -\frac{\rho_0 u_i u_r}{r}, \tag{A11b}$$

$$\frac{\partial}{\partial t_0}(\rho_0 u_i u_j + p\delta_{ij}) + \frac{\partial}{\partial x_l}[\rho_0 RT(u_i\delta_{jl} + u_j\delta_{il} + u_l\delta_{ij})] = -\frac{1}{\tau}\sum_\alpha f_\alpha^{(1)}\xi_{\alpha i}\xi_{\alpha j} - \frac{\rho_0 u_r}{r}RT\delta_{ij} \tag{A11c}$$

and

$$\frac{\partial}{\partial t_1}\rho_0 = 0, \tag{A12a}$$

$$\frac{\partial}{\partial t_1}(\rho_0 u_i) + \frac{\partial}{\partial x_j}\sum_\alpha f_\alpha^{(1)}\xi_{\alpha i}\xi_{\alpha j} = -\frac{2\tau\rho_0 RTu_r}{r^2}\delta_{ir} - \frac{1}{r}\sum_\alpha f_\alpha^{(1)}\xi_{\alpha i}\xi_{\alpha r}. \tag{A12b}$$

Neglecting the terms of high order in Mach number Ma, we have

$$\sum_\alpha f_\alpha^{(1)}\xi_{\alpha i}\xi_{\alpha j} = -\tau\left[\rho_0 RT\left(\frac{\partial u_i}{\partial x_j} + \frac{\partial u_j}{\partial x_i}\right) + \frac{\partial}{\partial t_0}(\rho_0 u_i u_j + p\delta_{ij})\right] = -\tau\rho_0 RT\left(\frac{\partial u_i}{\partial x_j} + \frac{\partial u_j}{\partial x_i}\right) + O(\mathrm{Ma}^2) \tag{A13}$$

and the resulting macroscopic equations are

$$\frac{\partial u_i}{\partial x_i} + \frac{u_r}{r} = 0, \tag{A14a}$$

$$\frac{\partial}{\partial t}(\rho_0 u_i) + \frac{\partial}{\partial x_j}(\rho_0 u_i u_j + p\delta_{ij}) + \frac{\rho_0 u_i u_r}{r} = \frac{\partial}{\partial x_j}\left[\mu\left(\frac{\partial u_i}{\partial x_j} + \frac{\partial u_j}{\partial x_i}\right)\right] + \frac{\mu}{r}\left(\frac{\partial u_i}{\partial r} + \frac{\partial u_r}{\partial x_i}\right) - \frac{2\mu u_r}{r^2}\delta_{ir} + O(\mathrm{Ma}^2), \tag{A14b}$$

which demonstrates that the standard incompressible NS equations for axisymmetric flows can be recovered from the proposed model with second-order accuracy in Ma. In contrast, the macroscopic equations recovered from the Li *et al.* [7] model, i.e., Eq. (A10), are compressible with truncation errors of third order in Ma. However, as claimed by Dellar [57], the solutions of Eq. (A10), derived from the standard LB model, approximate the solutions of the incompressible NS equations with errors of $O(\mathrm{Ma}^2)$. Thereby, the compressibility errors arising from the proposed incompressible model and the original Li *et al.* [7] model are of the same order. Further analysis on this issue is provided in Appendix C by applying the equivalent moment system proposed by Junk [39] based on the NS scale.

## APPENDIX B

A similar Chapman-Enskog analysis procedure is applied to the Zhou [9] model. In particular, the source terms based on the centered scheme are expanded as

$$\theta(\boldsymbol{x} + \boldsymbol{\xi}_\alpha\delta t/2, t + \delta t/2) = \theta(\boldsymbol{x}, t) + \frac{\varepsilon}{2}\left(\frac{\partial}{\partial t} + \xi_{\alpha i}\frac{\partial}{\partial x_i}\right)\theta(\boldsymbol{x}, t) + O(\varepsilon^2), \tag{B1a}$$

$$F_i(\boldsymbol{x} + \boldsymbol{\xi}_\alpha\delta t/2, t + \delta t/2) = F_i(\boldsymbol{x}, t) + \frac{\varepsilon}{2}\left(\frac{\partial}{\partial t} + \xi_{\alpha i}\frac{\partial}{\partial x_i}\right)F_i(\boldsymbol{x}, t) + O(\varepsilon^2). \tag{B1b}$$

Then the LB equation in Ref. [9] is expanded as, for $\varepsilon^0$, $\varepsilon^1$, and $\varepsilon^2$, respectively,

$$f_\alpha^{(0)} = f_\alpha^{(\mathrm{eq})}, \tag{B2a}$$

$$\left(\frac{\partial}{\partial t_0} + \xi_{\alpha i}\frac{\partial}{\partial x_i}\right) f_\alpha^{(0)} = -\frac{1}{\tau} f_\alpha^{(1)} + w_\alpha \theta + \frac{w_\alpha}{RT} F_i \xi_{\alpha i}, \tag{B2b}$$

$$\frac{\partial}{\partial t_1} f_\alpha^{(0)} + \left(1 - \frac{1}{2\tau}\right)\left(\frac{\partial}{\partial t_0} + \xi_{\alpha i}\frac{\partial}{\partial x_i}\right) f_\alpha^{(1)} = -\frac{1}{\tau} f_\alpha^{(2)} - \frac{(2\tau - 1)\xi_{\alpha r}}{2\tau r} f_\alpha^{(1)}. \tag{B2c}$$

With the moment equations pertaining to the conventional standard LB model, i.e., Eq. (12), moments of above expanded equations are obtained as

$$\frac{\partial}{\partial t_0}\rho + \frac{\partial}{\partial x_i}(\rho u_i) = -\frac{\rho u_r}{r}, \tag{B3a}$$

$$\frac{\partial}{\partial t_0}(\rho u_i) + \frac{\partial}{\partial x_j}(\rho u_i u_j + p\delta_{ij}) = F_i, \tag{B3b}$$

$$\frac{\partial}{\partial t_0}(\rho u_i u_j + p\delta_{ij}) + \frac{\partial}{\partial x_l}[\rho RT(u_i\delta_{jl} + u_j\delta_{il} + u_l\delta_{ij})] = -\frac{1}{\tau}\sum_\alpha f_\alpha^{(1)}\xi_{\alpha i}\xi_{\alpha j} + \theta RT\delta_{ij}, \tag{B3c}$$

$$\frac{\partial}{\partial t_1}\rho = 0, \tag{B4a}$$

$$\frac{\partial}{\partial t_1}(\rho u_i) + \left(1 - \frac{1}{2\tau}\right)\frac{\partial}{\partial x_j}\sum_\alpha f_\alpha^{(1)}\xi_{\alpha i}\xi_{\alpha j} = -\frac{2\tau - 1}{2\tau r}\sum_\alpha f_\alpha^{(1)}\xi_{\alpha i}\xi_{\alpha r}. \tag{B4b}$$

The unknown moment in Eq. (B4b) is derived from Eq. (B3) as

$$\sum_\alpha f_\alpha^{(1)}\xi_{\alpha i}\xi_{\alpha j} = -\tau\left[\rho RT\left(\frac{\partial u_i}{\partial x_j} + \frac{\partial u_j}{\partial x_i}\right) + (F_i u_j + F_j u_i)\right], \tag{B5}$$

where the extra term is a direct result of the simplified forcing source term $\frac{w_\alpha}{RT}F_i\xi_{\alpha i}$, which excludes the second-order terms in contrast with the force expression in Eq. (55c). With the definition of $F_i$ in the Zhou [9] model $F_i = -\frac{\rho u_i u_r}{r} - \frac{2\mu u_r}{r^2}\delta_{ir}$, the extra term is one order smaller than $O(\mathrm{Ma}^2)$ and can be neglected. Therefore, the macroscopic equations recovered from Ref. [9] are

$$\frac{\partial}{\partial t}\rho + \frac{\partial}{\partial x_i}(\rho u_i) = -\frac{\rho u_r}{r}, \tag{B6a}$$

$$\frac{\partial}{\partial t}(\rho u_i) + \frac{\partial}{\partial x_j}(\rho u_i u_j + p\delta_{ij}) = \frac{\partial}{\partial x_j}\left[\mu\left(\frac{\partial u_i}{\partial x_j} + \frac{\partial u_j}{\partial x_i}\right)\right] + \frac{\mu}{r}\left(\frac{\partial u_i}{\partial r} + \frac{\partial u_r}{\partial x_i}\right) + F_i, \tag{B6b}$$

where the dynamic viscosity is defined as $\mu = \rho(\tau - \frac{1}{2})RT\delta t$. Again, the standard NS equations for incompressible axisymmetric flows can also be obtained by applying the modified moments in Eq. (46) to Eq. (B2).

## APPENDIX C

In order to investigate the relationship between the LB equation and the incompressible NS equation, the NS scale (i.e., diffusive scale), which is distinct from the Boltzmann equation (BE) scale, was applied by Junk [39]. In both cases, the physical length $L$ is adopted as the representative space scale, but the velocity scales differ in that the lattice speed $c$, which relates to the sound speed $c_s$ by $c_s = c/\sqrt{3}$, is the typical speed for the BE scale, whereas the macroscopic speed $U$ serves as the velocity scale in the NS scale. Under the incompressible limit, the Mach number $\mathrm{Ma} = U/c_s$ satisfies the relationship [39,58]

$$U/c_s \sim U/c = \epsilon \sim \delta x/L. \tag{C1}$$

As a direct consequence of Eq. (C1), the representative time of the BE scale $T_{\mathrm{BE}} = L/c$ is one order $\epsilon$ smaller than that of the NS scale $T_{\mathrm{NS}} = L/U$, i.e., $T_{\mathrm{BE}} = \epsilon T_{\mathrm{NS}}$. Thus, the scaled time step $\Delta t = \delta t/T$ and spatial step $\Delta x = \delta x/L$ for these two scales have the relationships

$$\Delta t_{\mathrm{BE}} = \frac{\delta t}{T_{\mathrm{BE}}} = \frac{\delta x}{L} = \Delta x, \tag{C2a}$$

$$\Delta t_{\mathrm{NS}} = \frac{\delta t}{T_{\mathrm{NS}}} = \epsilon\frac{\delta t}{T_{\mathrm{BE}}} = \epsilon\frac{\delta x}{L} = \Delta x^2. \tag{C2b}$$

In the following, with the scaled quantities of $\tilde{\boldsymbol{x}} = \boldsymbol{x}/L$, $\boldsymbol{e}_\alpha = \boldsymbol{\xi}_\alpha/c$, and $\tilde{t} = t/T_{\mathrm{NS}}$ and scaled distribution function of $\tilde{f}_\alpha(\tilde{\boldsymbol{x}},\boldsymbol{e}_\alpha,\tilde{t}) = f_\alpha(L\tilde{\boldsymbol{x}},\boldsymbol{\xi}_\alpha,T_{\mathrm{NS}}\tilde{t})$, the scaled density function $\tilde{\rho}$ and scaled velocity function $\tilde{\boldsymbol{u}} = \boldsymbol{u}/\epsilon$ can be analogously defined (with $\epsilon = U/c$ and $c = 1$ in the present work), Thus,

the scaled LB equation is obtained as

$$\tilde{f}_\alpha(\tilde{\boldsymbol{x}}+\epsilon\boldsymbol{e}_\alpha,\boldsymbol{e}_\alpha,\tilde{t}+\epsilon^2)-\tilde{f}_\alpha(\tilde{\boldsymbol{x}},\boldsymbol{e}_\alpha,\tilde{t}) = -\frac{1}{\tau}\big[\tilde{f}_\alpha(\tilde{\boldsymbol{x}},\boldsymbol{e}_\alpha,\tilde{t})-\tilde{f}_\alpha^{(\mathrm{eq})}(\tilde{\rho}(\tilde{\boldsymbol{x}},\tilde{t}),\epsilon\tilde{\boldsymbol{u}}(\tilde{\boldsymbol{x}},\tilde{t});\boldsymbol{e}_\alpha)\big]. \quad \text{(C3)}$$

It should be noted that the complicated source terms accounting for the axisymmetric condition can be excluded in the present analysis since they would not affect the overall truncation error terms. Eliminating the tildes, the LB equation in the diffusion scaling (i.e., $\Delta t=\Delta x^2=\epsilon^2$) is given as

$$f_\alpha(\boldsymbol{x}+\boldsymbol{e}_\alpha\Delta x,\boldsymbol{e}_\alpha,t+\Delta t)-f_\alpha(\boldsymbol{x},\boldsymbol{e}_\alpha,t) = -\frac{1}{\tau}[f_\alpha(\boldsymbol{x},\boldsymbol{e}_\alpha,t)-f_\alpha^{(\mathrm{eq})}(\rho(\boldsymbol{x},t),\epsilon\boldsymbol{u}(\boldsymbol{x},t);\boldsymbol{e}_\alpha)]. \quad \text{(C4)}$$

Applying Taylor expansion around $\Delta t=\Delta x=0$ and neglecting the terms of order $\epsilon^2$ and higher, we have

$$\frac{\partial f_\alpha}{\partial t}+\frac{e_{\alpha k}}{\epsilon}\frac{\partial f_\alpha}{\partial x_k} = -\frac{1}{\epsilon^2\tau}\big(f_\alpha-f_\alpha^{(\mathrm{eq})}\big)+\frac{1}{2}e_{\alpha k}e_{\alpha l}\frac{\partial^2 f_\alpha}{\partial x_k\partial x_l} +\frac{1}{\epsilon\tau}e_{\alpha k}\frac{\partial}{\partial x_k}\big(f_\alpha-f_\alpha^{(\mathrm{eq})}\big) +\frac{1}{3}\epsilon e_{\alpha k}e_{\alpha l}e_{\alpha m}\frac{\partial^3 f_\alpha}{\partial x_k\partial x_l\partial x_m}, \quad \text{(C5)}$$

which is referred to as the modified Boltzmann equation and differs from the standard Boltzmann equation under the diffusive scaling

$$\frac{\partial f_\alpha}{\partial t}+\frac{e_{\alpha k}}{\epsilon}\frac{\partial f_\alpha}{\partial x_k} = -\frac{1}{\epsilon^2\tau}\big(f_\alpha-f_\alpha^{(\mathrm{eq})}\big). \quad \text{(C6)}$$

In order to transform Eq. (C5) to the equivalent moment systems, which is closer to the NS equations, a transformation matrix composed of nine scaled velocity polynomials is introduced as [39]

$$\boldsymbol{Q}=(Q_0,Q_1,\ldots,Q_8)^\dagger, \quad \text{(C7)}$$

where the dagger denotes the transpose operation and the specific basis vectors $Q_i(\boldsymbol{e}_\alpha)$ are given as

$$Q_0(\boldsymbol{e}_\alpha)=1, \quad \text{(C8a)}$$
$$Q_1(\boldsymbol{e}_\alpha)=e_{\alpha x}/\epsilon, \quad \text{(C8b)}$$
$$Q_2(\boldsymbol{e}_\alpha)=e_{\alpha y}/\epsilon, \quad \text{(C8c)}$$
$$Q_3(\boldsymbol{e}_\alpha)=(e_{\alpha x}^2-\tfrac{1}{3})/\epsilon^2, \quad \text{(C8d)}$$
$$Q_4(\boldsymbol{e}_\alpha)=e_{\alpha x}e_{\alpha y}/\epsilon^2, \quad \text{(C8e)}$$
$$Q_5(\boldsymbol{e}_\alpha)=(e_{\alpha y}^2-\tfrac{1}{3})/\epsilon^2, \quad \text{(C8f)}$$
$$Q_6(\boldsymbol{e}_\alpha)=(3|\boldsymbol{e}_\alpha|^2-4)e_{\alpha x}/\epsilon^3, \quad \text{(C8g)}$$
$$Q_7(\boldsymbol{e}_\alpha)=(3|\boldsymbol{e}_\alpha|^2-4)e_{\alpha y}/\epsilon^3, \quad \text{(C8h)}$$
$$Q_8(\boldsymbol{e}_\alpha)=(9|\boldsymbol{e}_\alpha|^4-15|\boldsymbol{e}_\alpha|^2+2)/\epsilon^4. \quad \text{(C8i)}$$

Similar to the basis given by Eqs. (48) and (49), the velocity polynomials are mutually orthogonal with respect to $w_\alpha$, i.e.,

$$\langle Q_i(\boldsymbol{e}_\alpha)Q_j(\boldsymbol{e}_\alpha)w_\alpha\rangle=\sum_\alpha Q_i(\boldsymbol{e}_\alpha)Q_j(\boldsymbol{e}_\alpha)w_\alpha=0 \quad \text{for } i\neq j. \quad \text{(C9)}$$

Then a linear invertible mapping from the distribution function space to the relevant moment space $|f\rangle\rightarrow\boldsymbol{M}$ is defined as

$$\boldsymbol{M}=\boldsymbol{Q}|f\rangle=(\langle Q_0 f\rangle,\langle Q_1 f\rangle,\ldots,\langle Q_8 f\rangle)^\dagger, \quad \text{(C10a)}$$
$$|f\rangle=\boldsymbol{Q}^{-1}\boldsymbol{M}=\sum_{j=0}^{8}\frac{M_jQ_j(\boldsymbol{e}_\alpha)}{\langle Q_j^2(\boldsymbol{e}_\alpha)w_\alpha\rangle}w_\alpha, \quad \text{(C10b)}$$

where $|f\rangle=(f_0,f_1,\ldots,f_8)^\dagger$ and $\boldsymbol{M}=(M_0,M_1,\ldots,M_8)^\dagger$ are the distribution function and moment column vector, respectively. With the transformation defined in Eq. (C10a), the moment equations pertaining to the standard Boltzmann equation [i.e., Eq. (C6)] are obtained as

$$\frac{\partial}{\partial t}M_0+\frac{\partial}{\partial x}M_1+\frac{\partial}{\partial y}M_2=0, \quad \text{(C11a)}$$
$$\frac{\partial}{\partial t}M_1+\frac{\partial}{\partial x}M_3+\frac{\partial}{\partial y}M_4+\frac{1}{3\epsilon^2}\frac{\partial}{\partial x}M_0=0, \quad \text{(C11b)}$$
$$\frac{\partial}{\partial t}M_2+\frac{\partial}{\partial x}M_4+\frac{\partial}{\partial y}M_5+\frac{1}{3\epsilon^2}\frac{\partial}{\partial y}M_0=0, \quad \text{(C11c)}$$
$$\frac{\partial}{\partial t}M_3+\frac{2}{3\epsilon^2}\frac{\partial}{\partial x}M_1+\frac{1}{3}\frac{\partial}{\partial y}M_7=-\frac{1}{\epsilon^2\tau}\big(M_3-M_3^{(\mathrm{eq})}\big), \quad \text{(C11d)}$$
$$\frac{\partial}{\partial t}M_4+\frac{1}{3\epsilon^2}\left(\frac{\partial}{\partial x}M_2+\frac{\partial}{\partial y}M_1\right)+\frac{1}{3}\left(\frac{\partial}{\partial x}M_7+\frac{\partial}{\partial y}M_6\right)=-\frac{1}{\epsilon^2\tau}\big(M_4-M_4^{(\mathrm{eq})}\big), \quad \text{(C11e)}$$
$$\frac{\partial}{\partial t}M_5+\frac{2}{3\epsilon^2}\frac{\partial}{\partial y}M_2+\frac{1}{3}\frac{\partial}{\partial x}M_6=-\frac{1}{\epsilon^2\tau}\big(M_5-M_5^{(\mathrm{eq})}\big). \quad \text{(C11f)}$$

The difference term between Eqs. (C5) and (C6),

$$\delta=\frac{1}{2}e_{\alpha k}e_{\alpha l}\frac{\partial^2 f_\alpha}{\partial x_k\partial x_l}+\frac{1}{\epsilon\tau}e_{\alpha k}\frac{\partial}{\partial x_k}\big(f_\alpha-f_\alpha^{(\mathrm{eq})}\big) +\frac{1}{3}\epsilon e_{\alpha k}e_{\alpha l}e_{\alpha m}\frac{\partial^3 f_\alpha}{\partial x_k\partial x_l\partial x_m}, \quad \text{(C12)}$$

leads to the following variations of the moment system in Eq. (C11):

$$\delta M_0=\frac{1}{6}\left(\frac{\partial^2}{\partial x^2}+\frac{\partial^2}{\partial y^2}\right)M_0+O(\epsilon^2), \quad \text{(C13a)}$$
$$\delta M_1=\frac{1}{\tau}\left(\frac{\partial}{\partial x}M_3^{(\mathrm{neq})}+\frac{\partial}{\partial y}M_4^{(\mathrm{neq})}\right)+\frac{1}{6}\Delta M_1 +\frac{1}{3}\frac{\partial}{\partial x}\left(\frac{\partial}{\partial x}M_1+\frac{\partial}{\partial y}M_2\right) +\frac{1}{9}\frac{\partial}{\partial x}(\Delta M_0)+O(\epsilon^2), \quad \text{(C13b)}$$

$$\delta M_2 = \frac{1}{\tau}\left(\frac{\partial}{\partial x}M_4^{(\mathrm{neq})} + \frac{\partial}{\partial y}M_5^{(\mathrm{neq})}\right) + \frac{1}{6}\Delta M_2 + \frac{1}{3}\frac{\partial}{\partial y}\left(\frac{\partial}{\partial x}M_1 + \frac{\partial}{\partial y}M_2\right) + \frac{1}{9}\frac{\partial}{\partial y}(\Delta M_0) + O(\epsilon^2), \tag{C13c}$$

$$\delta M_3 = \frac{1}{3\tau}\frac{\partial}{\partial y}M_7^{(\mathrm{neq})} + \frac{1}{9\epsilon^2}\frac{\partial^2}{\partial x^2}M_0, \tag{C13d}$$

$$\delta M_4 = \frac{1}{3\tau}\left(\frac{\partial}{\partial x}M_7^{(\mathrm{neq})} + \frac{\partial}{\partial y}M_6^{(\mathrm{neq})}\right) + \frac{1}{9\epsilon^2}\frac{\partial^2}{\partial x\partial y}M_0, \tag{C13e}$$

$$\delta M_5 = \frac{1}{3\tau}\frac{\partial}{\partial x}M_6^{(\mathrm{neq})} + \frac{1}{9\epsilon^2}\frac{\partial^2}{\partial y^2}M_0. \tag{C13f}$$

Neglecting the terms of order $\epsilon^2$ and higher, the evolution equations for the first three moment components, i.e., the equivalent moment system pertaining to the LB equation in diffusive scale, are derived as

$$\frac{\partial}{\partial t}M_0 + \frac{\partial}{\partial x}M_1 + \frac{\partial}{\partial y}M_2 = \frac{1}{6}\Delta M_0, \tag{C14a}$$

$$\frac{\partial}{\partial t}M_1 + \frac{\partial}{\partial x}M_3^{(\mathrm{eq})} + \frac{\partial}{\partial y}M_4^{(\mathrm{eq})} + \frac{1}{3\epsilon^2}\frac{\partial}{\partial x}M_0 = \frac{1}{3}\left(\tau - \frac{1}{2}\right)\Delta M_1 + \frac{\tau}{3}\frac{\partial}{\partial x}\left(\frac{\partial}{\partial x}M_1 + \frac{\partial}{\partial y}M_2\right) + \frac{2-\tau}{9}\frac{\partial}{\partial x}(\Delta M_0), \tag{C14b}$$

$$\frac{\partial}{\partial t}M_2 + \frac{\partial}{\partial x}M_4^{(\mathrm{eq})} + \frac{\partial}{\partial y}M_5^{(\mathrm{eq})} + \frac{1}{3\epsilon^2}\frac{\partial}{\partial y}M_0 = \frac{1}{3}\left(\tau - \frac{1}{2}\right)\Delta M_2 + \frac{\tau}{3}\frac{\partial}{\partial y}\left(\frac{\partial}{\partial x}M_1 + \frac{\partial}{\partial y}M_2\right) + \frac{2-\tau}{9}\frac{\partial}{\partial y}(\Delta M_0). \tag{C14c}$$

Applying the moment relationships for the standard LB method, the macroscopic equations are obtained as

$$\frac{\partial}{\partial t}\rho + \nabla\cdot(\rho\boldsymbol{u}) = \frac{1}{6}\Delta\rho, \tag{C15a}$$

$$\frac{\partial}{\partial t}(\rho\boldsymbol{u}) + \nabla\cdot(\rho\boldsymbol{u}\boldsymbol{u}) + \frac{1}{3\epsilon^2}\nabla\rho = \frac{1}{3}\left(\tau - \frac{1}{2}\right)\Delta(\rho\boldsymbol{u}) + \frac{\tau}{3}\nabla[\nabla\cdot(\rho\boldsymbol{u})] + \frac{2-\tau}{9}\nabla(\Delta\rho). \tag{C15b}$$

Introducing the order one function $p$, the density is decomposed as $\rho = \bar{\rho}(1 + 3\epsilon^2 p)$, where $\bar{\rho} > 0$ is the constant part. Thus, Eq. (C15) is rewritten as

$$\nabla\cdot\boldsymbol{u} = \frac{1}{6}\Delta(3\epsilon^2 p), \tag{C16a}$$

$$\frac{\partial}{\partial t}\boldsymbol{u} + \nabla\cdot(\boldsymbol{u}\boldsymbol{u}) + \nabla p = \frac{1}{3}\left(\tau - \frac{1}{2}\right)\Delta\boldsymbol{u} + \frac{2-\tau}{9}\nabla[\Delta(3\epsilon^2 p)]. \tag{C16b}$$

However, with the constant density assumption, the macroscopic equations pertaining to the proposed models are

$$\nabla\cdot\boldsymbol{u} = 0, \tag{C17a}$$

$$\frac{\partial}{\partial t}\boldsymbol{u} + \nabla\cdot(\boldsymbol{u}\boldsymbol{u}) + \frac{1}{\rho_0}\nabla p = \frac{1}{3}\left(\tau - \frac{1}{2}\right)\Delta\boldsymbol{u}. \tag{C17b}$$

Therefore, conclusions can be drawn from the present equivalent moment system based on the diffusive (NS) scaling that (i) the overall truncation errors of the LB equation in recovering the incompressible NS equation is second order in Ma ($\epsilon^2$) and (ii) the constant density assumption in the proposed incompressible models has the advantage of reducing the compressibility errors, as shown in the comparison between Eqs. (C15) and (C16) for the standard model and Eq. (C17) for the proposed incompressible models.

## APPENDIX D

The deviations of the computing formulas for the fluid pressure in the proposed models are provided in this appendix. Combining the modified second-order moments of the equilibrium distribution function and the results from the above Chapman-Enskog analysis, the second-order moment of the general distribution function is defined as

$$\sum_\alpha f_\alpha \xi_{\alpha i}\xi_{\alpha j} = \sum_\alpha \left(f_\alpha^{(\mathrm{eq})} + f_\alpha^{(\mathrm{neq})}\right)\xi_{\alpha i}\xi_{\alpha j} = \sum_\alpha \left(f_\alpha^{(0)} + \delta t f_\alpha^{(1)}\right)\xi_{\alpha i}\xi_{\alpha j} + O(\delta t^2). \tag{D1}$$

Substituting the moments of $f_\alpha^{(1)}$ for the proposed models, the second-order moment of the nonequilibrium part of the distribution is determined as

$$\sum_\alpha f_\alpha^{(\mathrm{neq})}\xi_{\alpha i}\xi_{\alpha j} = -\tau\rho_0 RT\left(\frac{\partial u_i}{\partial x_j} + \frac{\partial u_j}{\partial x_i}\right). \tag{D2}$$

Taking into account the definition of the reconstructed distribution function in Ref. [7]

$$\hat{f}_\alpha = f_\alpha - \frac{\delta t}{2}(\Omega_\alpha + S_\alpha),$$

we have

$$f_\alpha = \hat{f}_\alpha + \frac{\delta t}{2}(\Omega_\alpha + S_\alpha) \tag{D3}$$

and

$$\sum_{\alpha}\left(f_{\alpha}^{(\mathrm{eq})}+f_{\alpha}^{(\mathrm{neq})}\right)\xi_{\alpha i}\xi_{\alpha j} = \sum_{\alpha}\hat{f}_{\alpha}\xi_{\alpha i}\xi_{\alpha j}-\frac{1}{2\tau}\sum_{\alpha}f_{\alpha}^{(\mathrm{neq})}\xi_{\alpha i}\xi_{\alpha j}+\frac{\delta t}{2}\sum_{\alpha}S_{\alpha}\xi_{\alpha i}\xi_{\alpha j}. \tag{D4}$$

Applying the modified moments in Eq. (46) and the moment constraints in Eq. (D2), the fluid pressure in the incompressible model based on the Li *et al.* model [7] is determined as

$$p=\left(\sum_{\alpha}\hat{f}_{\alpha}\xi_{\alpha i}\xi_{\alpha i}-(2\tau+2)\delta t\rho_0 RT\frac{u_r}{r}-\rho_0\boldsymbol{u}^2\right)\Big/2, \tag{D5}$$

which is directly derived from the diagonal part of Eq. (D4). As for the incompressible model pertaining to the Zhou model [9], the computing formula of the fluid pressure is directly obtained from Eq. (D1),

$$\sum_{\alpha}f_{\alpha}\xi_{\alpha i}\xi_{\alpha j}=\rho_0 u_i u_j+p\delta_{ij}-\tau\rho_0 RT\left(\frac{\partial u_i}{\partial x_j}+\frac{\partial u_j}{\partial x_i}\right), \tag{D6}$$

which leads to

$$\sum_{\alpha}f_{\alpha}\xi_{\alpha i}\xi_{\alpha i}=\rho_0 u_i u_i+p\delta_{ii}-2\tau\rho_0 RT\frac{\partial u_i}{\partial x_i}, \tag{D7}$$

$$p=\left(\sum_{\alpha}f_{\alpha}\xi_{\alpha i}\xi_{\alpha i}-2\tau\delta t\rho_0 RT\frac{u_r}{r}-\rho_0\boldsymbol{u}^2\right)\Big/2. \tag{D8}$$


[1] R. S. Maier, R. S. Bernard, and D. W. Grunau, Phys. Fluids **8**, 1788 (1996).
[2] R. Mei, W. Shyy, D. Yu, and L.-S. Luo, J. Comput. Phys. **161**, 680 (2000).
[3] A. M. Artoli, A. G. Hoekstra, and P. M. A. Sloot, Int. J. Mod. Phys. C **13**, 1119 (2002).
[4] I. Halliday, L. A. Hammond, C. M. Care, K. Good, and A. Stevens, Phys. Rev. E **64**, 011208 (2001).
[5] T. S. Lee, H. Huang, and C. Shu, Int. J. Mod. Phys. C **17**, 645 (2006).
[6] T. Reis and T. N. Phillips, Phys. Rev. E **75**, 056703 (2007).
[7] Q. Li, Y. L. He, G. H. Tang, and W. Q. Tao, Phys. Rev. E **81**, 056707 (2010).
[8] J. G. Zhou, Phys. Rev. E **78**, 036701 (2008).
[9] J. G. Zhou, Phys. Rev. E **84**, 036704 (2011).
[10] Z. Guo, H. Han, B. Shi, and C. Zheng, Phys. Rev. E **79**, 046708 (2009).
[11] Q. Li, K. H. Luo, Q. J. Kang, Y. L. He, Q. Chen, and Q. Liu, Prog. Energy Combust. Sci. **52**, 62 (2016).
[12] F. Rong, Z. Guo, Z. Chai, and B. Shi, Int. J. Heat Mass Transfer **53**, 5519 (2010).
[13] L. Wang, Z. Guo, and C. Zheng, Comput. Fluids **39**, 1542 (2010).
[14] T. Zhang, B. Shi, Z. Chai, and F. Rong, Commun. Comput. Phys. **11**, 1569 (2012).
[15] H. Liang, Z. H. Chai, B. C. Shi, Z. L. Guo, and T. Zhang, Phys. Rev. E **90**, 063311 (2014).
[16] L. Zheng, B. Shi, Z. Guo, and C. Zheng, Comput. Fluids **39**, 945 (2010).
[17] L. Zheng, Z. Guo, B. Shi, and C. Zheng, J. Comput. Phys. **229**, 5843 (2010).
[18] T. Reis and T. N. Phillips, Phys. Rev. E **77**, 026703 (2008).
[19] T. Reis and T. N. Phillips, Phys. Rev. E **76**, 059902 (2007).
[20] H. Huang and X.-Y. Lu, Phys. Rev. E **80**, 016701 (2009).
[21] Y. Peng, C. Shu, Y. T. Chew, and J. Qiu, J. Comput. Phys. **186**, 295 (2003).
[22] H. Huang, T. Lee, and C. Shu, Int. J. Numer. Methods Fluids **53**, 1707 (2007).
[23] K. N. Premnath and J. Abraham, Phys. Rev. E **71**, 056706 (2005).
[24] S. Chen, J. Tölke, S. Geller, and M. Krafczyk, Phys. Rev. E **78**, 046703 (2008).
[25] S. Chen, J. Tölke, and M. Krafczyk, Phys. Rev. E **79**, 016704 (2009).
[26] T. S. Lee, H. Huang, and C. Shu, Int. J. Numer. Methods Fluids **49**, 99 (2005).
[27] S. Mukherjee and J. Abraham, Phys. Rev. E **75**, 026701 (2007).
[28] Q. Li, Y. L. He, G. H. Tang, and W. Q. Tao, Phys. Rev. E **80**, 037702 (2009).
[29] L. Li, R. Mei, and J. F. Klausner, Int. J Heat Mass Transfer **67**, 338 (2013).
[30] W. Xie, J. Comput. Phys. **281**, 55 (2015).
[31] H. Grad, Commun. Pure Appl. Math. **2**, 325 (1949).
[32] H. Grad, Commun. Pure Appl. Math. **2**, 331 (1949).
[33] X. Shan, X.-F. Yuan, and H. Chen, J. Fluid Mech. **550**, 413 (2006).
[34] L. S. Luo, W. Liao, X. Chen, Y. Peng, and W. Zhang, Phys. Rev. E **83**, 056710 (2011).
[35] P. Lallemand and L. S. Luo, Phys. Rev. E **61**, 6546 (2000).
[36] D. d'Humières, in *Rarefied Gas Dynamics: Theory and Simulations, Progress in Astronautics and Aeronautics*, edited by B. D. Shizgal and D. P. Weaver (AIAA, Washington, DC, 1994), p. 450.
[37] A. Montessori, M. La Rocca, G. Falcucci, and S. Succi, Int. J. Mod. Phys. C **25**, 1441003 (2014).
[38] A. Montessori, G. Falcucci, P. Prestininzi, M. La Rocca, and S. Succi, Phys. Rev. E **89**, 053317 (2014).
[39] M. Junk, Numer. Methods Part. D. E. **17**, 383 (2001).
[40] Z. Guo, C. Zheng, and B. Shi, Phys. Rev. E **65**, 046308 (2002).
[41] L. Zhang, Z. Zeng, H. Xie, Y. Zhang, Y. Lu, A. Yoshikawa, H. Mizuseki, and Y. Kawazoe, Comput. Math. Appl. **68**, 1446 (2014).
[42] L. Zhang, Z. Zeng, H. Xie, X. Tao, Y. Zhang, Y. Lu, A. Yoshikawa, and Y. Kawazoe, Comput. Math. Appl. **68**, 1107 (2014).
[43] P. J. Dellar, Physica A **362**, 132 (2006).
[44] P. J. Dellar, Phys. Rev. E **65**, 036309 (2002).
[45] R. Benzi, S. Succi, and M. Vergassola, Europhys. Lett. **13**, 727 (1990).
[46] R. Benzi, S. Succi, and M. Vergassola, Phys. Rep. **222**, 145 (1992).

[47] J. Latt, Ph.D. thesis, University of Geneva, 2007.
[48] A. J. Ladd, J. Fluid Mech. **271**, 285 (1994).
[49] A. J. Ladd, J. Fluid Mech. **271**, 311 (1994).
[50] G. Zhao-Li, Z. Chu-Guang, and S. Bao-Chang, Chinese Phys. **11**, 366 (2002).
[51] Z. L. Guo, C. G. Zheng, and B. C. Shi, Phys. Fluids **14**, 2007 (2002).
[52] Y. Wang, C. Shu, and C. J. Teo, Comput. Fluids **96**, 204 (2014).
[53] S. K. Bhaumik and K. N. Lakshmisha, Comput. Fluids **36**, 1163 (2007).
[54] K. Fujimura, H. S. Koyama, and J. M. Hyun, J. Fluids Eng. **119**, 450 (1997).
[55] M. Venkatachalappa, M. Sankar, and A. A. Natarajan, Acta Mech. **147**, 173 (2001).
[56] R. Iwatsu, Int. J. Heat Mass Transfer **47**, 2755 (2004).
[57] P. J. Dellar, J. Comput. Phys. **190**, 351 (2003).
[58] M. B. Reider and J. D. Sterling, Comput. Fluids **24**, 459 (1995).